Torben Carstensen

Design and optimization of a pitch-teeter coupling and the free teeter angle for a two-bladed wind turbine to reduce operating loads

Masterarbeit eingereicht im Rahmen der Masterprüfung

im Studiengang Nachhaltige Energiesysteme im Maschinenbau
am Department Maschinenbau und Produktion
der Fakultät Technik und Informatik
der Hochschule für Angewandte Wissenschaften Hamburg

in Zusammenarbeit mit:

aerodyn engineering gmbh
Hollerstraße 122
24782 Büdelsdorf

Erstprüfer: Professor Dipl.-Ing Peter Dalhoff
Zweitprüferin: M.Eng. Vera Schorbach

Industrieller Betreuer: M.Sc. Jan-Christoph Hinrichs

Abgabedatum: 08. Februar 2015

Zusammenfassung

Name des Studierenden
Torben Carstensen

Thema der Masterarbeit
Entwicklung und Optimierung einer Pitch-Pendel-Kopplung und des freien Pendelwinkels für eine Zweiblatt-Windenergieanlage zur Reduzierung der Betriebslasten

Stichworte
Wind, Lastsimulation, Betriebslasten, Ermüdungslasten, Pendelnabe, Delta-3, Pitch-Pendel-Kopplung, Pitch-Pendel-Koeffizient, Endanschlag, IEC 61400-1

Kurzzusammenfassung
Eine Möglichkeit die Stromgestehungskosten zu senken ist der Einsatz von Zweiblatt-Windenergieanlagen. Allerdings entstehen aufgrund der Rotorform höhere dynamische Kräfte an Zweiblattanlagen. Dem entgegenwirken kann man mit der Integration einer Pendelnabe. Besonders die Ermüdungslasten lassen sich damit stark reduzieren.
In dieser Arbeit werden die verschiedenen Parameter von Pendelnabe und Endanschlags auf den Einfluss auf die Ermüdungslasten hin untersucht und optimiert. Die Simulationen werden nach IEC 61400-1 durchgeführt.

Name of Student
Torben Carstensen

Master Thesis title
Design and optimization of a pitch-teeter coupling and the free teeter angle for a two-bladed wind turbine to reduce operating loads

Keywords
Wind, load simulation, operational loads, fatigue loads, teetering hinge, delta-3, pitch-teeter coupling, pitch-teeter coefficient, end stop, IEC 61400-1

Abstract
A possibility to reduce the cost of energy is the use of two-bladed wind turbines. However, the rotor design causes higher dynamic forces on two-bladed turbines, which can be counteracted using a teetering hinge. Especially the fatigue loads can be reduced significantly.
In this thesis the different parameters of teetering hub and end stop are analyzed and optimized for the fatigue loads. The simulations were conducted according to IEC 61400-1.

Contents

List of Figures

List of Tables

Chapter 1

Introduction

1.1 Motivation

The main objective for wind turbine manufacturer is to decrease the cost of energy of their turbines. On the onshore market, the turbine development reached already a high stage. Wind turbines are able to compete with conventional power plants depending on the site. However, current offshore wind parks have higher cost of energy caused by expensive transportation, installation and maintenance [21].

Because of this, a renunciation of the standard three-bladed design is discussed in the last years [7]. The construction of two-bladed wind turbines could have advantages especially for the offshore market. First of all, a reduction to a two-bladed rotor could decrease the total turbine costs. The rotor is generally one of the large cost drivers. Secondly, two-bladed turbines can be transported and installed easier and more cost-efficiently.

The poorer aerodynamic efficiency of a two-bladed rotor should be more than compensated that way, so that the cost of energy could be reduced overall [6, p.345]. Other disadvantages like higher noise level and a more disturbing rotor motion compared to a three-bladed wind turbine play a minor role for offshore installations.

Another disadvantage of a two-bladed turbine is that the rotor design induces large fluctuating out-of-plane bending moments in the rotor hub caused by wind shear. Due to the high number of load cycles in the lifetime of a wind turbine, these high bending moments have a strong influence on the fatigue damage [24].

Theoretically this loads can be eliminated if the rotor blades are not connected rigid to the shaft but pivot-mounted. When the whole rotor is mounted on a

hinge, the rotor is allowed to teeter down- and upwind. The aerodynamic forces that occur at the blades are not longer transferred in the main shaft and the following drive train, which would significantly reduce the fatigue loads.

In practice, the teeter motion is limited by the turbine design, so a maximal teeter angle must not be exceeded. Therefore, a teeter end impact reduces the kinetic energy of the rotor, which, however, causes additional bending moments in the hub and would raise the fatigue loads.

A possibility to reduce the teeter amplitude is the pitch-teeter coupling. In this case, the blades are pitched in dependence of the current teeter angle, which causes a restoring effect on the rotor, see figure 1.1. So on the one hand, a teetering hub can significantly reduce the fatigue loads of a two-bladed hub. On the other hand, the additional degree of freedom of the rotor causes a more complex rotor hub with a several parameters that influence the loads and the teeter motion.

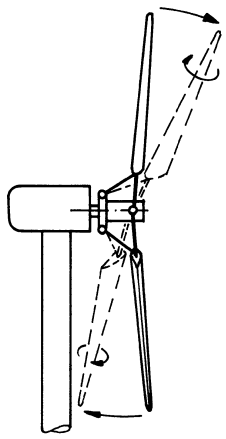

Figure 1.1: Pitch-teeter coupling [16, p.242]

1.2 Scope

The aim of this thesis is to develop a pitch-teeter coupling (PTC) for a two-bladed 3 MW wind turbine with teetered hub and analyze its influence on the teeter motion and on the fatigue loads. Two different methods to couple pitch and teeter motion are simulated. Secondly, the teeter end impact shall be optimized in order to reduce the fatigue loads. Therefore, different free teeter angles and spring-damper characteristics will be analyzed. The simulation results are focused mainly on the hub loads, especially the out-of-plane bending moments.

The simulation model will be simulated with the aerolastic simulation software Bladed. The research in this thesis is based on a validated wind turbine model, which includes a complete design load case definition according to the IEC guidelines.

1.3 About the research project ZOFF

This thesis is part of the research project ZOFF at the Hamburg University of Applied Sciences. ZOFF stands for "Zweiblatt-Offshore-Windenergieanlagen" (in engl.: two-bladed offshore wind turbines) and is running since 2011. It is concerned with the potential of two-bladed turbines related to the reduction of cost of energy. This shall be accomplished with evaluating and developing teetering concepts. The focus is on the load simulation of the hub and the teeter end impact [2].

The industry partner of this research project is aerodyn engineering gmbh. aerodyn provides the knowledge and data of the SCD3.0-100, which is the basis for the simulation model of this thesis. The SCD3.0-100 is a two-bladed 3 MW wind turbine and has a rigid hub. SCD stands for "Super Compact Drive". Generator, gear box and rotor bearing are in a compact housing, whereby the typical nacelle can be omitted.

Chapter 2

Fundamentals

2.1 Two-bladed wind turbines

The three-bladed wind turbine is the standard design of a modern wind turbine with horizontal rotor axis. However, there have been many developments of machines with two-bladed rotor in the past. Furthermore, it could be observed an increasing trend of new two-bladed projects in the recent years [7].

Cost of energy

The main argument to develop a two-bladed wind turbine is the possible reduction of cost of energy (CoE).

$$Cost\,of\,energy = \frac{Total\,costs}{Energy\,produced}$$

The total costs include the costs for the wind turbine, the costs for transport and installation as well as the annual operating costs. The produced energy is the added annual energy yield over the life time of the wind turbine.

Looking at the power output of a wind turbine, the missing blade can be compensated by increasing the chord width of the blades or by increasing the rotational speed of the turbine. But the power coefficient C_P would still be slightly smaller than the C_P of a three-bladed rotor, which will lower the energy yield, see figure 2.1.

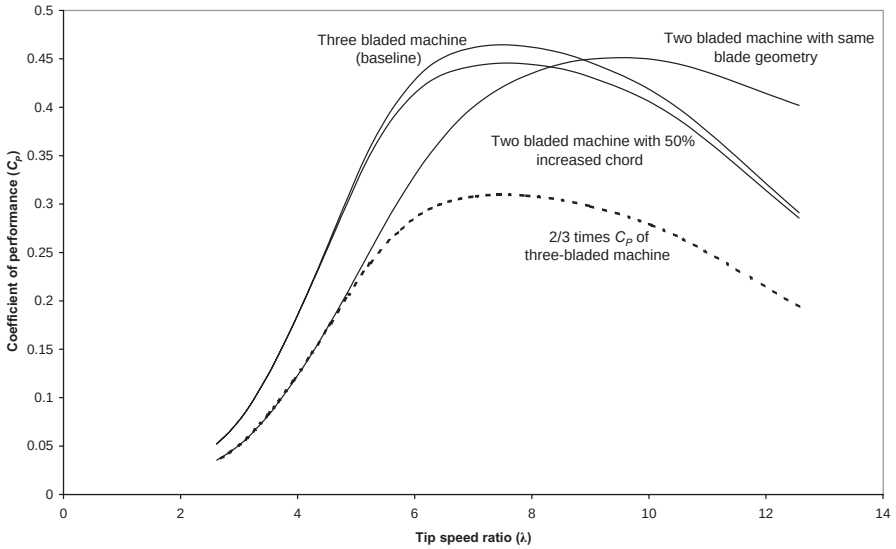

Figure 2.1: C_P-curves for two- and three-bladed rotors [6, p.344]

Costs can be saved in the turbine production. The weight and therefore the material costs decrease due to the elimination of one rotor blade. But the rotor costs do not decrease to 2/3 the cost of a three-bladed rotor by saving one blade. The blade reduction has an effect on other turbine components, too.

If the rotor chord increases, the blade needs to be reinforced to maintain the same level of solidity. This would raise the costs of one blade and negate possible savings.

If the rotor speed is increased, the costs for machine components, like hub and shaft for example, rise because of higher loads. However, the costs of other components like the drive train decrease because the transmitting torque would drop with increasing rotational speed, according to $P = T \cdot \omega$ [6, p.341-346]. A lower torque means less material and therefore less material costs, too.

On the other hand, costs can be saved during transportation and assembling, especially if it is an offshore turbine. The nacelle with fully assembled light rotor can be shipped from the harbour to the offshore wind farm. In the wind farm, nacelle and rotor can be mounted on the tower in one lift and so the operating time of vessels and workforce can be reduced.

Another benefit of an offshore installation is that the noise level as well as the unsmooth run of a two-bladed turbine is not important on the sea.

Fluctuating bending moments caused by asymmetric wind conditions

Fluctuating dynamic loads are a major drawback of two-bladed wind turbines. Assymetric wind conditions like wind shear have a larger impact on two-bladed than on three-bladed wind turbines. If the rotor is in vertical position, the loads are therefore larger on the upper than on the lower blade. This causes an out-of-plane bending moment in hub and shaft of the turbine. Due to the rotor rotation, the loads fluctuate once per rotor revolution (to rotating axis). Other forms of asymetric wind conditions appear in case of a yaw misalignment, for example, see figure 2.2 [26].

Different blade loads caused by asymmetric wind also exists at a three-bladed rotor, but here the loads can equalize each other in some extent due to the design [6, p.295].

Another difference is the change of mass of inertia. That means the two-bladed rotor has a different mass of inertia in the horizontal position than in the vertical. The dynamical rotor reaction caused by loads thus depends of the rotor position while a three-bladed rotor has a steady mass of inertia. This effect increases the bending moments even further [16, p.222].

The larger fluctuating bending moments in combination with the long operational time leads to larger fatigue loads in comparison to a three-bladed turbine.

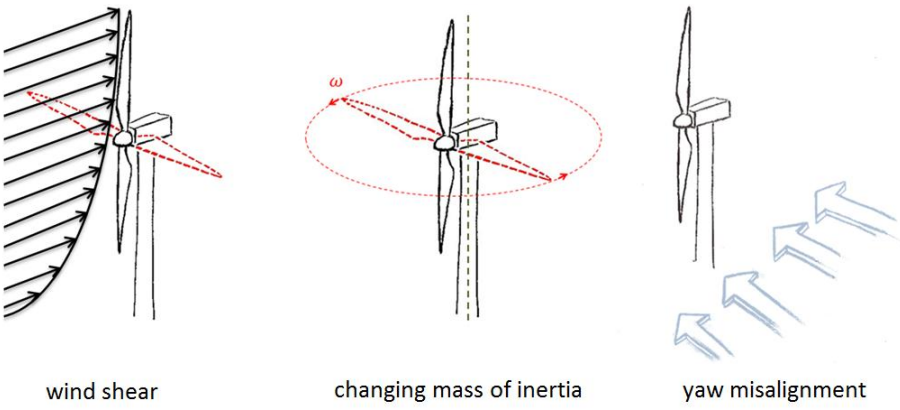

Figure 2.2: Sources of turbine loads [26]

2.2 Teetered hub

The effects of asymmetric wind conditions, which were mentioned above, are related to two-bladed turbines with a rigid hub. But the transmission of the blade

loads to the shaft can be prevented from those bending moments by a hinge with its axis perpendicular to shaft and rotor axis. As illustrated in figure 2.3 the rotor can teeter to compensate the different aerodynamic loads on the blades.

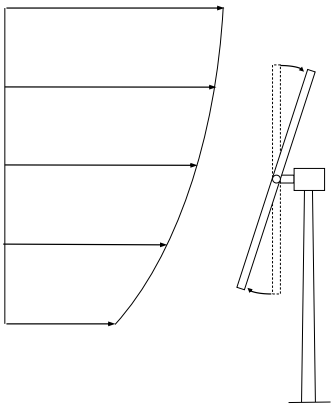

Figure 2.3: Teetering hub

2.2.1 Teeter motion

The simplified teeter motion can be described as a damped forced oscillation. The unequal blade loads causes a net moment M, which rotate the rotor around the teeter axis. Different influences act towards this motion. Besides the mass moment of inertia about the teeter axis J, also a restoring respectively restricting moment result from centrifugal forces and aerodynamic damping. The centrifugal force can be described as a stiffening with the coefficient k_{cf} , the aerodynamic damping with the damping coefficient C_a [27].

$$J \cdot \ddot{\zeta} + C_a \cdot \dot{\zeta} + k_{cf} \cdot \zeta = M(t) \tag{2.1}$$

The lateral ratio of the centrifugal force is in this case the restoring moment of the teeter movement. The higher the rotor speed, the higher the restoring moment. Also the mass of the rotor influences the centrifugal force, whereby the stiffness ratio k_{cf} can be described with

$$k_{cf} = J \cdot \Omega^2 \tag{2.2}$$

The aerodynamic damping depends, on the one hand, on the chord length c and the air density ρ [6, p. 271]. Thus, the larger the chord, the larger the rotor surface

and the larger the air resistance. On the other hand, the angle of attack and the lift affect the damping, too. At high angle of attack, the airflow can separate from the airfoil (stall), which causes a lift drop. This can eliminate the aerodynamic damping at all. The relation is described as

$$C_a = \frac{1}{2} \cdot \rho \cdot \Omega \cdot C_{l\alpha} \cdot \int_{-R}^{+R} c(r) \cdot |r| \cdot r^2 dr \tag{2.3}$$

where r is the rotor radius and $C_{l\alpha}$ the gradient of the lift curve $\frac{\mathrm{d}C_l}{\mathrm{d}\alpha}$ [27]. In case of stall $C_{l\alpha}$ is zero or negative. [22, p.190]

Without the external moment and damping, the motion can be described as a free teeter oscillation

$$J \cdot \ddot{\zeta} + J \cdot \Omega^2 \cdot \zeta = 0 \tag{2.4}$$

Therefore, the natural frequency of the teeter motion ω_{Teeter} would be equal to the rotational frequency Ω, with $\omega_{Teeter} = \sqrt{\frac{k}{J}}$. Because the bending moment from aerodynamic loads depends on the rotor position and also on the rotor frequency, the system would operate in resonance without the aerodynamic damping [6, p. 271].

2.2.2 Teeter end impact

Due to the additional degree of freedom, the rotor can theoretically collide with the tower or the nacelle, when the teeter angle ζ is large enough. This would happen especially when the restoring and resisting forces of the teeter motion are low. During a start-up or a shut down of the wind turbine, the rotor speed is low and thus also the restoring centrifugal force, for example [24].

To prevent a contact, a maximum teeter angle ζ_{max} has to be determined, which must not be exceeded. Therefore, a teeter end impact is required. This is a system of spring and/or damping elements in the hub area, which shall reduce the kinetic energy of the teeter motion. They are defined with k_h and C_h respectively. This leads to additional loads on the turbine, which can eliminate the advantages of a teetering hub. Due to the additional kinetic energy of the teeter motion the resulting loads can even be higher than the loads of a equivalent turbine with rigid hub [24]. Therefore, a configuration of the restraint parameters has always to be a compromise.

The end impact needs a teeter range ζ_{EI} to operate. For that reason, the teeter system is devided in specific teeter angles. The beginning of the end impact is also the end of the free teetering and is defined as the free teeter angle ζ_{free}, see figure 2.4.

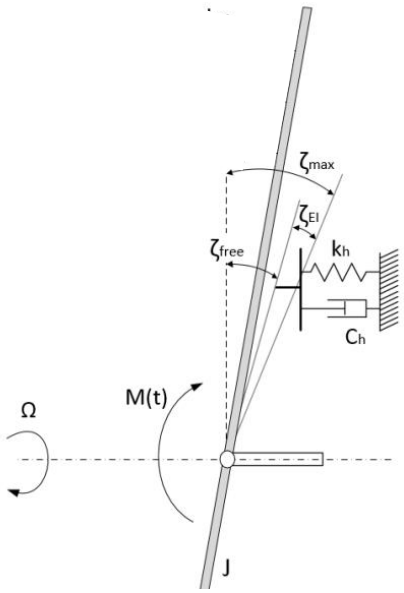

Figure 2.4: Teeter end impact layout [29, modified]

2.2.3 Delta-3 coupling

A solution to reduce the teeter excursions is the coupling of pitch angle and teeter angle. This can be done by different techniques.

One method is to rotate the hinge axis around the shaft axis in rotor plane. So the teeter hinge axis and the blade axis are not perpendicular anymore. The angle between the primary position and the rotated axis of the teeter hinge is called δ_3 (delta-3) [22, p.290f].

Figure 2.5 shows a teetering hub with a delta-3 angle. It should be noted that this is a design for a downwind rotor. The blue line is perpendicular to the blade axis. It is also called aerodynamic teeter axis. The orange line is rotated by the delta-3 angle about the shaft axis. This axis is also called delta-3 axis or mechanical teeter axis.

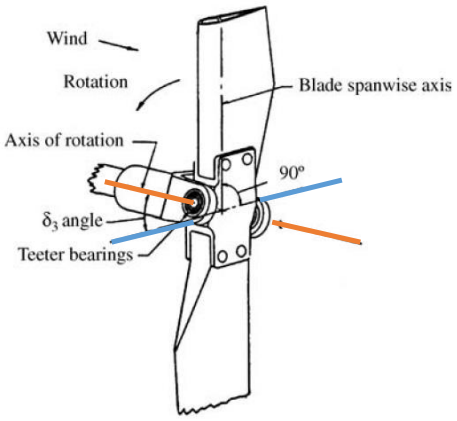

Figure 2.5: Teetering hub with delta-3 axis [22, p.292, modified]

The delta-3 axis affects an additional pitch at the blades in opposite directions. As an example: When a higher thrust acts at blade A than at blade B, blade A teeters in downwind direction and pitches in positive direction (out of the wind) while blade B teeters in upwind direction and pitches in negative direction. The lift at blade A is thereby reduced, while it was raised at blade B. This circumstance counteracts the teeter movement.

The hinge design is also called delta-3 coupling. The larger the delta-3 angle, the larger the change in pitch angle. The mathematical connection of the pitch change $\Delta\beta$ and the teeter angle ζ is described as follows:

$$\Delta\beta = \zeta \cdot \tan(\delta_3) \tag{2.5}$$

where the element $tan(\delta_3)$ can also called pitch-teeter coefficient C_{pt}:

$$C_{pt} = \tan(\delta_3) \tag{2.6}$$

A special case occurs at a delta-3 angle of 45 deg. The pitch-teeter coefficient is $C_{pt} = 1$ and thus teeter angle and pitch change are equal.

Because the delta-3 axis stiffens the teeter system, the pitch-teeter coupling can also described as a spring coefficient k_a. Therefore, the parameter has to be considered in the oscillation equations (2.1) and (2.4), which means that also the natural frequency of the teeter system is changed.

It is shown in [6, p. 273] that the natural frequency ω_{Teeter} is shifted by changing the hinge axis as follows:

$$\omega_{Teeter} = \Omega \cdot \sqrt{1 + \frac{1}{8}\gamma \cdot C_{pt}} \tag{2.7}$$

where γ is the Lock number.

The Lock number is the ratio of aerodynamic forces to inertial forces. $C_{l\alpha}$, which was decribed in section 2.2.1, is also included in the Lock number. So if the aerodynamic forces do not influence the calculation (e.g. in case of stall), the Lock number is $\gamma = 0$ [22, p. 190].

Equation (2.7) shows, that the natural frequency of the teeter motion ω_{Teeter} is raised by a positive pitch-teeter coefficient.

Considering all parameters of section 2.2.2 and 2.2.3, (2.1) can be extended to

$$J\ddot{\zeta} + (C_a + C_h)\dot{\zeta} + (k_{cf} + k_a + k_h)\zeta = M(t) \tag{2.8}$$

The influence of the different parameters on the teeter motion is visualized in figure (2.6).

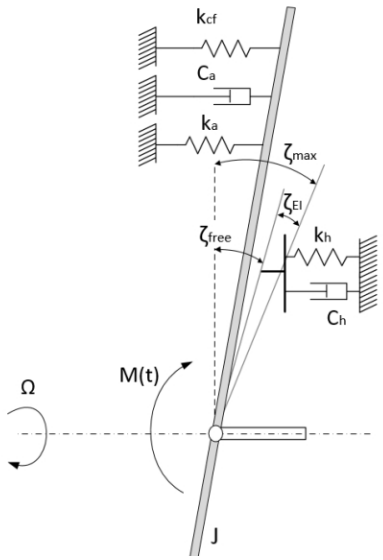

Figure 2.6: Parameters of teeter oscillation [29]

2.2.4 Active pitch-teeter coupling

A pitch-teeter coupling can also be provided by a lever or gear mechanism. An advantage of this method is the possibilty of a variable pitch-teeter coefficient C_{pt}

whereas the delta-3 angle is fixed according to the construction [16, p. 290f]. A more modern approach is to connect pitch and teeter motion via the pitch controller. The teeter angle is measured, is multiplied with the pitch-teeter coefficient C_{pt} and is transferred to the pitch actuator as demand signal. This has the same advantages as the mechanical method but without the connection of levers or gears.

2.2.5 Teeter lock

For a stable teeter motion the restoring moments due to centrifugal forces are very important. But in situations like turbine start up or shut down, the rotor speed is lower and therefore the centrifugal forces, too. The results are high teeter amplitudes and high loads caused by the teeter end stop [24]. To prevent this case, a teeter lock was provided in the wind turbines developed in the past, which should lock the rotor motion about the teeter axis if the rotor speed is too low or the turbine is parked.

2.3 Concepts with teetering hub

2.3.1 Concepts in the past

At the beginning of the development of modern wind turbines all projects had the same problem. The wind energy was too expensive to compete against the low oil price. So the investment in wind energy technology was poor, which is why only single prototypes often existed. An example is the two-bladed wind turbine with teetering hub developed by Hütter. This downwind turbine with a power of 100 kW was regarded as a trend-setter even several years later. But also the project of Hütter ended due to financial problems [30, p.105ff].

First the oil crisis in the 80s changed this situation. Research projects were started in many countries to study alternative energies and to become independent of oil. Therefore, large research wind turbines with an output power in the MW-range were developed in the USA, Germany and Sweden amongst others [16, p.45].

It should be mentioned that most of the turbines were designed with two-bladed rotors. A third blade was regarded to be not cost-effective. The turbine concepts differed a lot in case of turbine design and turbine control [28].

Two of the research projects are described below:

The WTS-4 was a two-bladed downwind turbine that was developed within the research project of the United States. The machine was placed in operation in 1982 and had an output power of 4 MW. A teetering rotor with a delta-3 axis of 30 degree integrated. Because the rotor was coned with 6 degree, the teeter axis was not located at the intersection of the blade and rotor axis but was located inside the defined coned form. This moves the teeter axis closer to the center of gravity of the rotor, which prevents a drift away from the neutral position [12, p.5].

The result of the German research project was the wind turbine Growian, which was erected also in 1982. It has a capacity of 3 MW power and was deemed to be the most modern wind turbine at that time. Growian was also designed as a downwind turbine with a teetered two-bladed rotor and a pitch-teeter coupling. In contrast to the WTS-4, the pitch-teeter coupling was realized by a lever mechanism. The pitch-teeter coefficient could be varied between 1 and 2.5 [16, p.291].

The operation of the research turbines resulted in new and important knowledge about the dynamical turbine behavior, but it showed off the technical limits, too. Many of the project turbines could not fulfill the expectations and had to be dismantled much earlier than expected caused by component failures. One of the major reasons was the high number of load cycles, which caused fatigue. Furthermore, the computer technology was not sufficiently advanced to simulate the turbulent wind and the turbine dynamics accurately enough. The consequence was often a too weak design of the turbine components.

The wind turbine Growian for example had to be dismantled after a lifetime of approximately 400h. The main cause was a failure in the development of the teetering hub design. During start-ups and shutdowns high loadings appear caused by the teeter impacts. The hub, a welded steel frame, was not strong enough to resist such high loadings, which results in cracks in the construction [16, 29].

2.3.2 Current projects

Two-bladed turbines could not be established yet despite the large research turbines. Also with the beginning of building offshore wind farms most of the turbine designer remain with the classical proven three-bladed design. A change to a two-bladed rotor is in contrast financielly risky. An example is Nordic Windpower. They developed and sold a 1 MW turbine with a teetered hub, but went bankrupt in 2012 [20]. Furthermore, the range of different two-bladed concepts is still large [28].

Two of the current MW-range projects are described below:

The Vergnet GEV HP 1MW is a two-bladed upwind turbine with an output power of 1 MW. This concept was developed especially for areas with difficult terrain and poor infrastructure. A special feature is the integrated erection tool, which can be used to lift nacelle and rotor in one step. Lowering the nacelle can be used, to perform turbine service at ground level or as storm protection. The rotor is connected with the shaft over a teetering hub. Also a delta-3 axis is integrated. According to figure 2.7, the delta-3 angle is beyond 60 deg.

Figure 2.7: Vergnet's delta-3 axis [23]

Condor Wind Energy is a designer of a two-bladed wind turbine, which was especially developed for offshore conditions. The Condor 6 has a output power of 6 MW and a teetering hinge without pitch-teeter coupling. The teeter hinge is designed as a T-shaped shaft with two elastomeric bearings. The teeter range differs between 2 and 4 deg. The small range is adjusted for wind speeds below rated. With increasing wind speed, the restriction for teeter motion is reduced. The 4 deg teeter range is adjusted for cut out wind speed. As shown in figure 2.8 the rotor blades are rigidly mounted on the hub. So a pitch control is not considered. Instead, the turbine is regulated via an active yaw control.

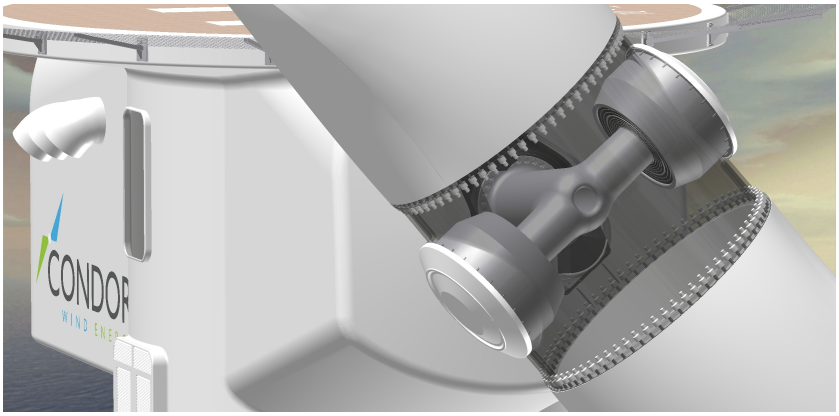

Figure 2.8: Condor 6 teetered hub [1]

2.4 SCD3.0-100

The simulation model, which is used in this thesis, is based on the wind turbine SCD3.0-100 developed by aerodyn engineering gmbh. It is a two-bladed upwind turbine with a rigid hub and a rotor diameter of 100 m. SCD stands for Super Compact Drive, which is a unique feature of this turbine. The rotor bearing is integrated in the drivetrain and the frames of gearbox and generator are also the housing of the nacelle. Therefore, the turbine does not contain a machine bed or a common external housing, see figure 2.9.

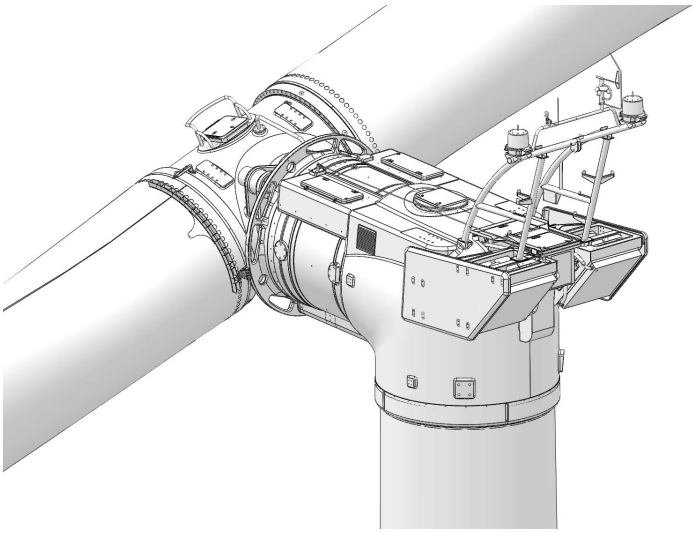

Figure 2.9: SCD3.0-100 turbine head [5]

The SCD3.0-100 is part off the SCD onshore series, which contains also models for low wind and nearshore conditions. The offshore series includes turbines with 6 to 8 MW power, also in SCD design.

A data sheet to the SCD3.0-100 is illustrated in table 2.1.

Table 2.1: SCD3.0-100 data sheet [5]

Description	Unit	Specifation
Drive train		
Rated power	kW	3000
Speed control	-	By blade pitch
Operational mode	-	Variable speed
Rotor		
Rotor type	-	Two-bladed, upwind
Rotor diameter	m	100
Hub height	m	85
Tilt angle	deg	5
Generator		
Genearotor type	-	Permanent magnet synchronous
Wind speed limits		
Mean wind speed	m/s	8.5
Cut-in speed (10 min means)	m/s	3.0
Rated wind speed	m/s	12.9
Cut-out speed (10 min means)	m/s	25.0

The technological advances in the turbine development is most evident if the head masses of the presented wind turbines (rotor with blades inclusive) are compared, see table 2.2. The German research turbine Growian had a head mass of about 400 t. The SCD3.0-100 has in contrast a head mass of about 100 t, but with the same output power. Today the turbine components can be designed accurately to the load conditions due to a computer-aided turbine development. This can reduce weight but also turbine loads. Therefore the SCD3.0-100 does not need any additional pitch-teeter coupling for load reduction.

But it is also shown in the comparison of Condor 6 and SCD3.0-100 that an increasing turbine power leads to a disproportional rise of the head mass. The

mass difference between the SCD3.0-100 and SCD 6.0 is even larger (200 t).

With increasing weight it is more difficult to withstand the occurring loads. Therefore, a pitch-teeter coupling is perhaps needed in future developments.

Table 2.2: Head mass comparison

Turbine	Power [kW]	Head mass [t]
Growian	3000	≈ 400
Vergnet GEV HP1000	1000	64
Condor 6	6000	256
SCD3.0-100	3000	≈ 108

The SCD3.0-100 has the lowest rotational speed in comparison to the current two-bladed turbines with teetering hub, see table 2.3. The rotational speed influences the aerodynamic forces, which control the teeter amplitude, see equation (2.5).

Table 2.3: Rotational speed comparison

Turbine	Rotational speed [rpm]
Vergnet GEV HP1000	23.0
Condor 6	19.4
SCD3.0-100	17.1

SCD3.0-100 with teetered hub

The design of the teetering hub is not part of the scope, but some teetering hub parameters had to be defined for the simulations.

Due to the small teeter amplitudes and the high number of load cycles, conventional plain- or rolling element bearings would wear prematurely. Elastomeric bearings are known as fatigue endurable, which is why those were used in the teeter concepts in the past and would be used for the teeter bearing of the SCD.

Caused by the basic characteristics of an elastomeric bearing, the teeter motion would be stiffened and damped. So a spring and a damping coefficient have to be considered in the free teeter range. The teeter end stop should start at a teeter angle of 3.5 deg and should be designed as a spring with a linear rate. The maximal allowable teeter angle is 6 deg.

2.5 Load calculation

A wind turbine is a complex building, which consists of various high stressed and moving components. The turbine loads result from wind, gravity and centrifugal forces. Different models are needed to evaluate these loads.

- A model of the wind conditions
- A model of the aerodynamic at the rotor blades
- A model of the structural dynamics of the turbine

2.5.1 Wind model (IEC 61400-1)

It is attempted to simulate realistic wind situations. Steady wind conditions are therefore not sufficient. Because the turbulence of the wind causes additional fluctuations in the turbine loads, a turbulent wind model is important especially concerning fatigue loads.

The wind model, which was used in this thesis, is based on the IEC 61400-1 Edition 3. This guideline is published by the International Electrotechnical Commission and is part of a collection of international standards for design requirements for wind turbines. There are different wind conditions defined in the IEC 61400-1, which depend on the wind turbine class, hub height and rotor diameter.

Wind shear

The wind shear, which was mentioned before, is considered with (2.9). The power law exponent α is assumed to be 0.2.

$$V(z) = V_{hub}(z/z_{hub})^{\alpha} \tag{2.9}$$

The parameters are:

$V(z)$	Wind speed at height z
V_{hub}	Wind speed at hub height
z_{hub}	Hub height

Turbulence intensity TI

The normal turbulence model (NTM) was defined to represent the wind condition that usually occurs at the wind site. This model is used to evaluate the fatigue loads.

The wind speed varies around a mean wind speed. The variation of the wind speed is characterized in the NTM by a standard deviation σ_1, which is calculated with

$$\sigma_1 = I_{ref} \cdot (0.75 \cdot V_{hub} + b) \tag{2.10}$$

The parameters are:

I_{ref}	Defined reference turbulence intensity
b	Constant (= 5.6 m/s)

The turbulence intensity TI is the quotient of the standard deviation and the wind speed at hub height. The relationship of (2.11) is illustrated in figure 2.10.

$$TI = \frac{\sigma_1}{V_{hub}} \tag{2.11}$$

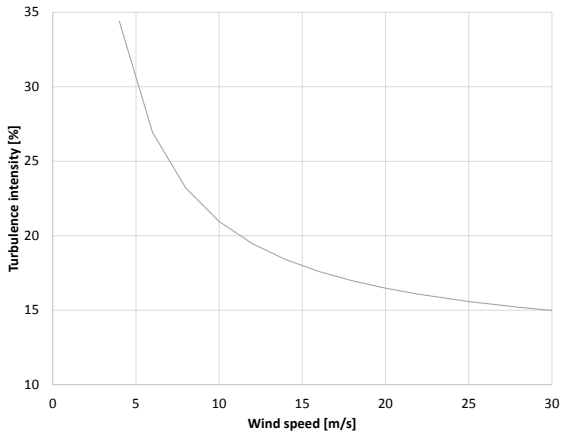

Figure 2.10: Turbulence intensity over wind speed

Three dimensional turbulence model

The wind speed varies in all three dimensions. Therefore, a three dimensional turbulence model is needed.

The model is a rectangular grid of points. The grid area has to cover the rotor area completely. On every gridpoint, the wind speed is variating over the time, but with a defined mean wind speed.

The wind speed "is generated for each of these points in such a way that each time history has the correct single-point turbulence spectral characteristics, and each pair of time histories has the correct cross-spectral or coherence characteristics" [10, p.88].

There are different approaches to simulate the wind turbulence. The mathematical context is explained in [10, p.88ff].

An example of a point in a three dimensional turbulence time history is shown in figure (2.11). This picture illustrates very well the grid model, turbulence and wind shear.

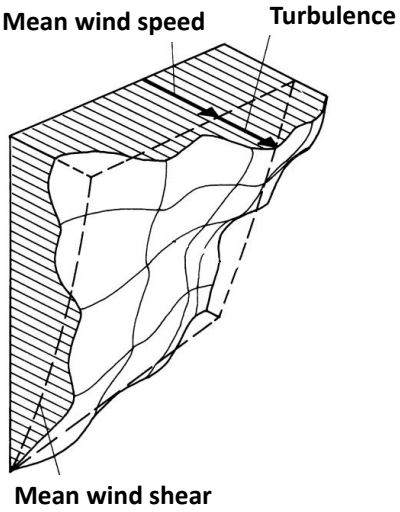

Figure 2.11: 3D turbulence model [16, p.215, modified]

2.5.2 Aerodynamic model (BEM)

The most common used aerodynamic model is the blade element momentum theory, which is a combination of the momentum theory and the blade element theory.

The momentum theory is also called actuator disc model. In this model, the wind turbine rotor is modeled as a infinitely thin disc in a stream tube of air. The air is flowing through the rotor and is losing therefore kinetic energy. The flow is stationary, incompressible and frictionless. There is also no energy or mass transfer through the stream tube boundary [22, p.92].

Due to the kinetic energy loss, the air slows down behind the rotor disc. With the assumption made, the mass flow $\dot{m}$ of the air has to be constant, see equation (2.12) and 2.13. The air stream therefore expands behind the disc. So the downstream flow has a larger cross-section than the upstream flow, see figure 2.12.

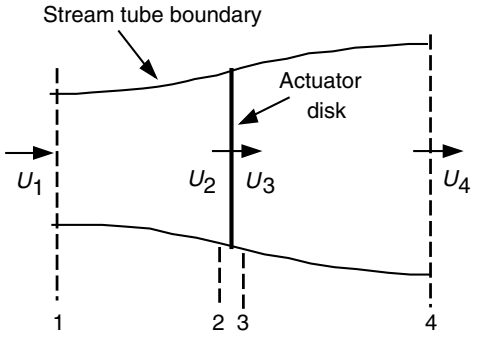

Figure 2.12: Actuator disc model [22, p.93]

$$\dot{m}_1 = \dot{m}_2 = \dot{m}_3 = \dot{m}_4 \tag{2.12}$$

$$\rho \cdot A_1 \cdot U_1 = \rho \cdot A_2 \cdot U_2 = \rho \cdot A_3 \cdot U_3 = \rho \cdot A_4 \cdot U_4 \tag{2.13}$$

The thrust T, which is the force of the wind on the rotor disc, is caused by the pressure drop over the rotor. The extracted wind power P is then equal to the thrust T times the wind speed at the disc U_2.

$$T = A_2 \cdot (p_2 - p_3) \tag{2.14}$$

$$P = A_2 \cdot (p_2 - p_3) \cdot U_2 \tag{2.15}$$

A flow induction factor a is defined in this model, which describes the relationship between the velocities U_1 and U_2 [10, p.6].

$$U_2 = U_1 \cdot (1 - a) \tag{2.16}$$

With the factor a and the Bernoulli function, equation (2.14) and (2.15) can also described with

$$T = \frac{1}{2} \cdot \rho \cdot A \cdot U^2 \cdot [4a \cdot (1 - a)] \tag{2.17}$$

and

$$P = \frac{1}{2} \cdot \rho \cdot A \cdot U^3 \cdot 4a \cdot (1 - a)^2 \tag{2.18}$$

Here, the wind speed U_1 is replaced with U and the disc area A_2 is replaced with A [10, p.7].

This model does not consider the torque Q yet. The extracted power P is a product of the torque Q and the angular velocity of the rotating rotor Ω. Due to actio = reactio, it is a angular momentum of the air flow required, which is equal and opposite to the a torque developed by the rotor. Therefore, a tangential velocity is induced to the flow.

The angular velocity of the air flow ω_{air} is defined by the angular flow induction factor a'.

$$a' = \frac{\omega_{air}}{2 \cdot \Omega} \tag{2.19}$$

The torque Q generated by the rotor is

$$Q = \pi \cdot \rho \cdot R^4 \cdot (1 - a) \cdot a' \cdot U \cdot \Omega \tag{2.20}$$

In the blade element theory, the rotor disc is devided into N annuli, which are swept out by each blade element, see figure 2.13.

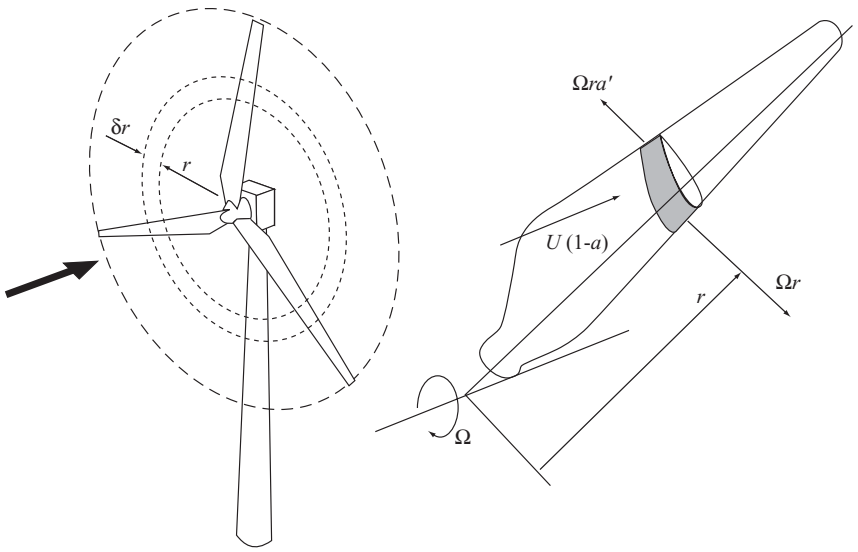

Figure 2.13: Rotor disc devided in annuli [6, p.60]

Every annulus can be treated like the rotor disc above because it is assumed that the annuli are radial independent. Thrust T and torque Q can be calculated therefore

$$dT = 4\pi \cdot r \cdot \rho \cdot U^2 \cdot a \cdot (1 - a)\, dr \tag{2.21}$$

and

$$dQ = 4\pi \cdot r^3 \cdot \rho \cdot U \cdot \Omega \cdot a \cdot (1 - a) \cdot a'\, dr \tag{2.22}$$

The forces at each blade element can also be calculated by the two-dimensional aerofoil characteristics, see figure 2.14.

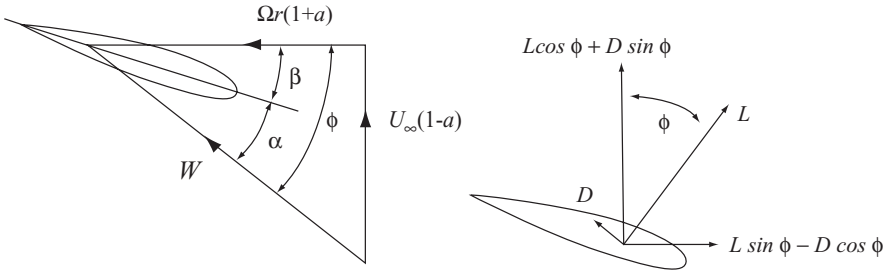

Figure 2.14: Blade element velocities and forces [6, p.61]

The relative velocity W and the angle of attack α result from wind speed and rotational speed. The forces of a profile, lift and drag, act tangential and normal respectively to the relative flow direction. They are determined with the specific drag and lift coefficient of the aerofoil, C_l and C_d respectively:

$$L = \frac{1}{2} \cdot \rho \cdot W^2 \cdot c \cdot C_l \tag{2.23}$$

$$D = \frac{1}{2} \cdot \rho \cdot W^2 \cdot c \cdot C_d \tag{2.24}$$

with chord length c.

With the projection in the direction of thrust and torque and the regard to the number of blades, the forces can be insert in formula (2.21) and (2.22) to calculate the induction factors a and a'.

All this information is sufficient to determine the resulting forces.

2.5.3 Model of structural dynamics (Multi-body)

An additional model is needed to simulate the effect of the aerodynamic forces on the turbine components. The multi-body dynamics approach is a possible method.

The rigid components are described as interconnected nodes, see figure 2.15. Every node has a specific number of degrees of freedom (DOF). External loads act directly at the nodes [10, p.15f].

With the principle of virtual work all forces, displacements, stiffness and damping values can be summarized in a matrix system, according to equation 2.25 .

$$M\ddot{x} + C\dot{x} + Kx = F_g \tag{2.25}$$

The larger the number of DOF, the higher the computational time to solve the matrix system. To keep the solving time low, the flexible components, rotor blade and tower, are described as beam elements with two nodes at the ends and defined mass and stiffness. The deflection can be described by pre-calculated modal shape functions. They are calculated from the eigenmodes of the finite element model of the flexible structure [10, p.16f].

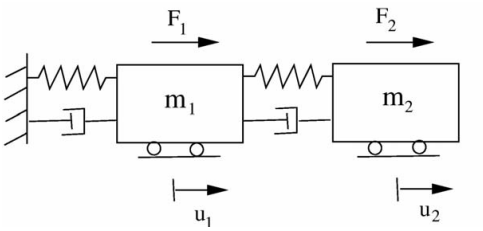

Figure 2.15: DOF system [15, p.132]

2.6 Simulation tool Bladed

Bladed is an aerolastic simulation software developed by Garrad Hassan. In this thesis, version 4.5 was used.

Bladed combines the three models explained in section 2.5. Therefore, Bladed provides to define turbine parameters like rotor and tower dimension, but also the control- and electrical system. The wind conditions can be defined as well as the sea state in case of an offshore turbine.

In addition to the aerodynamic BEM model, Bladed considers different empirical approaches to improve the results [10, p.9]. Furthermore, it is a special feature that the theoretical methods in Bladed have been validated against monitored measurements from a wide range of real wind turbines [10, 31].

Different coordinate systems are used in Bladed. The coordinate system for the hub loads are based on the convention of the Germanischen Lloyd and is shown in figure 2.16 . The x-axis is along the shaft axis and is pointing to the tower. The z-axis is perpendicular to the x-axis and is pointing vertically upwards. The y-axis is the resultant axis to make a right-handed coordinate system. Different to figure 2.16, the z-Axis is in line with the axis of blade 1. Furthermore, the used co-ordinate system is fixed to the rotor and rotates according to the rotor rotation.

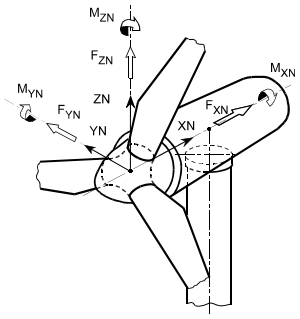

Figure 2.16: Coordinate system for hub loads [11]

2.7 Power production control

To build up a realistic simulation model in Bladed, also the power control of the turbine has to be adopted. The SCD3.0-100 is a variable speed pitch regulated turbine. An advantage of this control model is that below rated wind speed the rotor speed is not fix, but can be adjusted in a way that the optimum tip-speed ratio λ_{opt} is yielded. At this tip-speed ratio the power coefficient C_P is maximized.

The rotor speed or the generator speed, respectively, is controlled by the generator torque Q_g. So Q_g has to be set in order to reach always the optimal tip-speed ratio. With (2.26) the aerodynamic torque Q_a is given. The gear box ratio and the mechanical losses in the drive train are known. So the optimum generator torque can be calculated for different rotor speeds [6, p.481f].

$$Q_a = \frac{1}{2} \cdot \rho \cdot \pi \cdot R^5 \cdot \frac{C_P}{\lambda^2} \cdot \Omega^2 \tag{2.26}$$

The result is the line B-C in figure 2.17 .

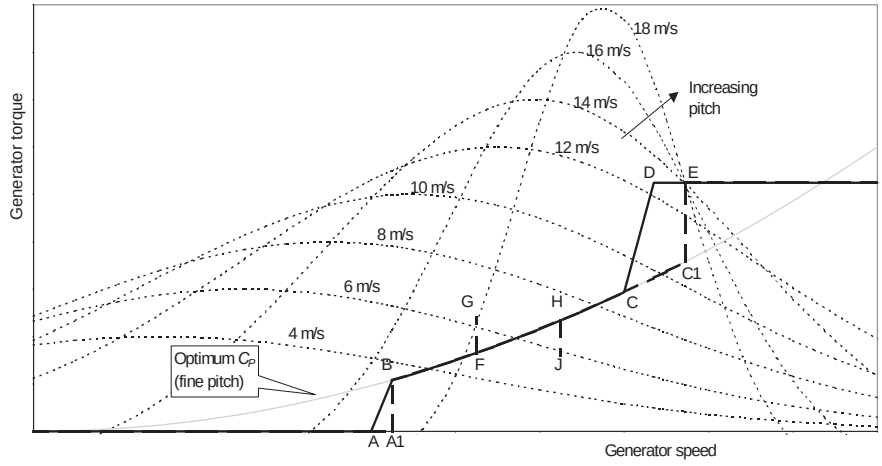

Figure 2.17: Torque-speed curve [6, p.482]

This principle could be continued till the rated generator torque is reached. But because high rotor speed causes also high loads, it is usual to increase the torque instead of the rotor speed. This is considered with the torque-speed ramp C-D.

To prevent a possible further increasing of the generator speed at rated generator torque, the pitch control is used at point E of figure 2.17 . By pitching the blades, the aerodynamic efficiency can be decreased, which decreases the aerodynamic torque, too. The result is a deceleration of the rotor.

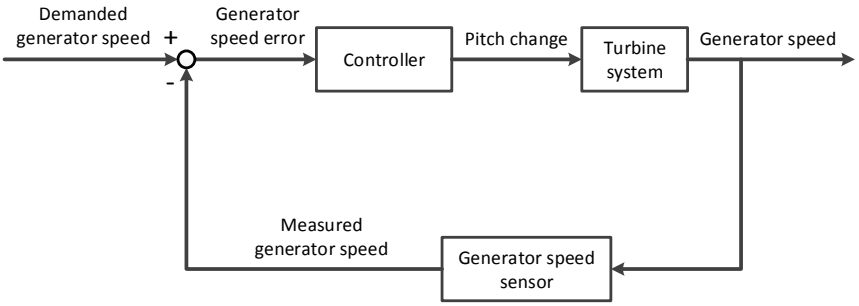

Figure 2.18: Closed-loop pitch control

Because of the turbulent character of the wind, the pitch angle has to respond rapidly to the current wind conditions. The pitch control is therefore designed as a closed-loop control, see figure 2.18. The difference between the actual measured generator speed and the demanded generator speed is the control error e, which is the input value for the controller. The general approaches of the control theory are used for this pitch controller. The different algorithms are briefly described below [25]. The output signal of the pitch-controller is the pitch change, which is dedicated to the pitch actuators. The change of pitch angle leads to a changing aerodynamic rotor torque and therefore to a changing generator speed. In figure 2.18 this process is simplified and summarized under the term turbine system. The process could actually be described more complex. A pitch actuator has its own closed-loop control to set the correct pitch angle, for example.

Proportinal term

The error e is multiplied with the parameter K_p. So the output pitch change is proportional to the current error.

$$\Delta\beta(t) = K_p \cdot e(t) \tag{2.27}$$

Integral term

The integral term sums the error e up over the time as long as the error is present. The summed error is multiplied with the gain factor K_i. So the longer the error exist, the larger is the output value $\Delta\beta$.

$$\Delta\beta = K_i \cdot \int_0^t e(\tau)d\tau \tag{2.28}$$

Derivative term

The derivative term analysis the gradient of the error over the time and multiplies it with the factor K_d. So if the difference between demand and measured value raises faster, the output value $\triangle\beta$ increases. The derivative term has the fastest response of the three described terms, but can also leads to a disturbed control behavior.

$$\Delta\beta = K_d \cdot \frac{\mathrm{d}e(t)}{\mathrm{d}t} \tag{2.29}$$

The described terms can be combined [6, p.505]. The aim is to reduce the calculated error e. A wrong adjustment of the tuning parameters K_p, K_d und K_i could for example lead to overshoots. The generator speed would oscillate around the target speed.

2.8 Fatigue analysis

Structural elements that are subjected to oscillating loads may fail after a certain number of cycles, although the loads are under the tensile strengths of the element. This effect is known as the fatigue damage [13].

Load cases

Because of the high number of load cycles during the lifetime of a wind turbine, the fatigue damage is a main design driver for the development. For the calculation all load cycles has to be considered. So the aim of the load calculation has to be to determine all occuring fatigue loads.

The following fatigue load cases are recommended by the IEC:

- Power production with normal turbulent wind NTM - DLC 1.2
- Power production plus occurrence of faults with NTM - DLC 2.4
  - The fault should be a normal power production at maximum yaw error [14, p.107].

- Start up with steady wind conditions NWP - DLC 3.1
- Normal shut down with NTM - DLC 4.1
- Parked with NTM - DLC 6.4
  - Two-bladed wind turbines are usually parked in horizontal rotor position with a pitch angle of 90 deg.

This load cases cover almost all load cycles during life time. Extreme events, which are needed for the calculation of the extreme loads, occur very rarely and thus do not affect the fatigue damage. For that reason, they are not considered for the fatigue analysis.

The recommended design load cases shall be simulated at different wind speeds over a period of 10 minutes. Because not every load case or wind speed appear equally often, it is assumed that the incidence of the wind speeds follow a Rayleigh distribution [8, p.144]. The results of the 10-minute-simulations can now be extrapolated to the assumed life time of 20 years [18].

Rainflow counting

The simulation results are given as time series with varying loads and have to be prepared for the fatigue analysis. Different counting algorithms are used to count and sort the load cycles. The rainflow counting algorithm is one of them. It is common used in the wind turbine development and is therefore also applied in Bladed.

The counting requires a time series only with maxima and minima loads. Furthermore, the load scale is separated in several load classes and the load cycles have to be separated into single load hysteresis. Two of those with the same amplitude, but opposite oscillation direction, make a closed load hysteresis. The definition of a closed hysteresis can be explained with the stress-strain diagram, see figure 2.19.

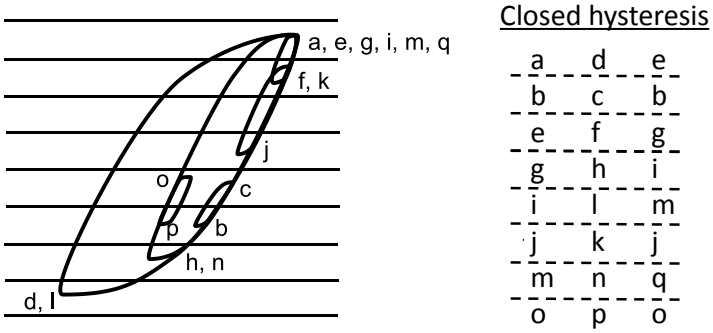

Figure 2.19: Closed hysteresis in a stress-strain diagram [19, p.24, modified]

The closed load hysteresis are sorted by cycle range and are counted. The result could be presented as a stepped fatigue load spectrum for the total life time. Every step i has a defined cycle range L_i and a number of cycles n_i.

If, for example, two different turbine configurations should be compared with each other, the fatigue load spectra differs in cycle range and load cycle number. A simple graphical comparison is not possible.

The load spectra have to be converted into damage equivalent loads L_{equi} according to equation (2.30). The number of cycles n_i is therefore scaled to a reference value n_{ref} [3].

$$L_{equi} = \sqrt[m]{\frac{\sum(n_i \cdot L_i)}{n_{ref}}} \tag{2.30}$$

Factor m depends on material and geometry of the structural component. It is provided by the turbine designer, as well as the reference number of cycles n_{ref}.

- $m = 4$
- $n_{ref}= 1 \cdot 10^7$

Figure 2.20 shows a example of a load spectrum and its damage equivalent load. The load cycle has been separated in $i = 128$ load steps.

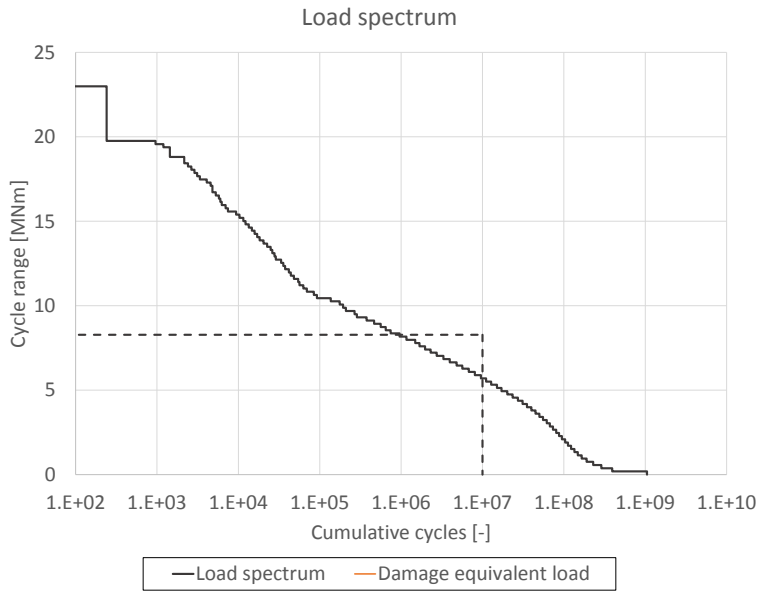

Figure 2.20: Example of a load spectrum and the damage equivalent load

Chapter 3

Simulation model

The simulation model is based on the SCD3.0-100. Due to the realization of a teetering hinge, the rotor hub would be designed differently. Thus, the layout of the pitch actuators that are located in the hub would be changed, too.

A construction of a teetering hub is not considered in the scope of this thesis. It is assumed that the implementation of the teetering hub does not influence the turbine parameters.

It was not necessary to build up a whole new simulation model in Bladed for this thesis. It could be used the SCD3.0-100 model that was already developed and desribed in [14]. A validation of this Bladed model was also done there. The results have been compared to the results of the aerolastic simualtion tool aeroflex, which is developed and used by aerodyn. The validation resulted in a large deviation for the hub My moment that could not be reduced. For that reason, the topic is raised in section 3.1.

The wind model was built up in Bladed according to the IEC. The precise description of the model details are discussed in [14].

3.1 Validation with aeroFlex

aeroFlex is a aerolastic simulation tool like Bladed. The program code of aeroFlex is based on the simulation software FLEX5, which was developed at the Technical University of Denmark. The main differences to Bladed are listed below:

- aeroFlex uses only a modal approach instead of a combination with finite elements.

- Bladed uses a pitching moment coefficient whereas this is not considered in aeroFlex. The pitching moment coefficient shall consider a moment about the blade axis caused by the air flow at the airfoil. But because this moment should be close to zero for the most cases, the consequence of a non-consideration should be marginal.
- Another difference lies in the assumption of the blade forces. In both simulation tools, the forces are calculated at discrete blade segments. However, in aeroFlex, the calculated forces at a segment are assumed to be constant in the section around the blade segment. So the blade loads are sectionwise constant with load steps between. In Bladed, the forces for the sections between the discrete blade segments are interpolated linearly.
- The co-ordinate systems differ in the orientation of the axis. The x- and z-axes are switched and the y-axis has the opposite orientation.

To validate the developed Bladed model, the simulation results have been compared to the results of an aeroFlex turbine model. It was noticed that the hub My loads differed up to 128.6 % in [14, p.38], while the divergence of the other loads was in an acceptable range. A solution for this disparity was not found at that time.

Therefore, further researches have been done as part of this thesis. The simulation loads have been determined in simplified load cases. In table 3.1 the maximum and minimum hub loads are compared for a wind speed of 14 m/s. In this example, no yaw misalignment or mass- and pitch imbalances are used. The results are compared in table 3.1. The differences are declared in relative values, according to equation (3.1).

Table 3.1: Comparison of the hub loads

Load	Min. value [%]	Max. value [%]
Mx	+ 0.44	+ 8.32
My	+ 54.50	+ 53.45
Mz	- 1.49	- 1.21
Fx	+ 1.02	- 7.25
Fy	+ 0.71	+ 0.82
Fz	- 0.06	- 0.06

$$x = \left(\frac{x_{Bladed} - x_{aeroFlex}}{x_{aeroFlex}} - 1 \right) \cdot 100 \tag{3.1}$$

All results, except the hub My loads, are in an acceptable range. The shown divergence increases at lower wind speeds.

It was assumed that the divergence is caused by the blade loads. Therefore, the blade root loads have been compared, too. It is shown in table 3.2 that the relative deviation is increased for the blade My, Mz and Fx root loads. In case of Mz and Fx, the absolute values are small in comparison to the My loads. For that reason, a small absolut difference could result in a larger relative deviation.

The difference in blade My loads are increased, but not in the same rate as the hub My loads. But this is misleading, too. The hub My load is the resultant of the two blade My root loads. If the hub My load is calculated according to (3.2), the result is similar to the value in 3.1. So the large deviation of the hub My loads can be attributed to the blade root loads.

$$My_{Hub} = My_{Blade1} - My_{Blade2} \tag{3.2}$$

The shown divergence could not be decreased significantly during the thesis. It could not be found any mistake in the simulation model, which has such a large influence on the loads.

In spite of this phenomenon, the simulation model will be used for the following researches. If different teetering hub configurations are compared to each other, the possible mistake will be included in every single result. The result of the comparisons will not be affected.

Table 3.2: Comparison of the blade 1 root loads

Load	Min. value [%]	Max. value [%]
Mx	+ 0.33	+ 9.71
My	+ 4.21	- 12.23
Mz	+ 14.77	- 15.63
Fx	+ 3.09	- 12.19
Fy	+ 2.93	+ 1.35
Fz	- 0.61	- 1.17

3.2 Teeter restraint

Theoretically, the out of plane moments can be removed completely with a teetered hub. But in practice the teeter amplitude has to be limited. Thus, out of plane moments still occur when reaching the end stop. The torque level depends on the teeter restraint characteristic of the end stop.

The Bladed user interface allows defining the torque caused by the teeter restraint via a look-up table. Therefore, non-linear stiffness of the end stop can be described, too. Values between the points of the look-up table are interpolated linearly.

The maximal allowable teeter angle was determined to 6 deg by the turbine designer. So the first goal was to find a linear stiffness, for which the maximal teeter angle does not exceed this threshold in every DLC. The limit of free teetering was set to 3.5 deg in the first design.

The result was a restraint stiffness of 6109 $\frac{\text{kNm}}{\text{deg}}$ with a maximal teeter angle of 5.89 deg.

The restraint curve is illustrated in figure 3.1. The stiffness of the free teeter section is non-zero caused by the stiffness of the teeter bearing. The characteristic of the restraint system is identical for the positive and negative section.

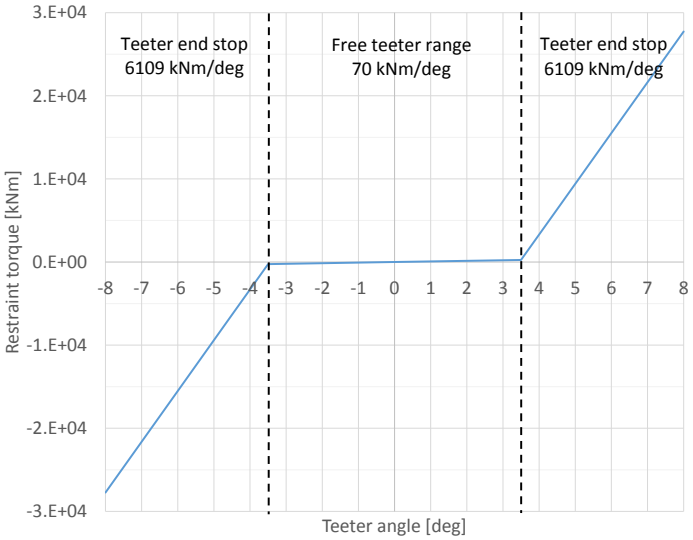

Figure 3.1: Teeter restraint characteristic

The Bladed interface also allows the definition of a teeter damping. A damping

ratio $D_{teeter} = 0.06$ was determined by a manufacturer of elastomeric bearings to consider the friction in the teeter bearing.

Bladed only allows the definition of the damping coefficient c_h, which can be determined with equation 3.3. The restraint system characteristic is summarized in table 3.3.

$$c_h = \frac{2 \cdot D_{teeter} \cdot k_h}{\omega} \tag{3.3}$$

The parameters are:

c_h Damping coefficient

D Damping ratio

k_h Spring stiffness

ω Natural frequency of the system (rotor speed)

Table 3.3: Teeter restraint characteristic

	Range [deg]		Teeter restraint	
	From	To	Spring rate $\left[\frac{\text{kNm}}{\text{deg}}\right]$	Damping coefficient [kNms]
Free	0.0	3.5	70	$2.69 \cdot 10^5$
Stop	3.5	6	6109	

3.3 Implementation of the pitch-teeter coupling

A delta-3 coupling can be activated via the Bladed interface. The delta-3 angle is freely adjustable. The active PTC, however, can not be defined this way. The coupling of pitch and teeter motion has to be controlled by an external controller, which is described in the following section.

3.4 External controller

Bladed enables to define the different aspects of the turbine control system over the Bladed user interface. Regarding to the pitch control settings, the possible setting options are not sufficient to simulate the wind turbine behavior on an appropriate level.

First, Bladed enables only the use of a PI controller. But for the control model of the SCD3.0-100 a controller with PD behavior is required to get realistic simulation results.

Second, to implement an electromechanical pitch-teeter coupling, as described in section 2.2.4, the controller needs the ability to control the two pitch actuators individually. Bladed can't meet these two requirements via the user interface. Another possibility is to integrate a user-defined controller, which can take over some or all functions of the built-in controllers. This user-defined controller has to be a DLL (dynamic link library), but can be written in different languages [9].

aerodyn provided such a controller DLL for this thesis, which was already used in [14]. However, the controller DLL didn't support individual pitch control and could not be extended.

Therefore, a simple controller was written for this thesis to enable the definition of the major functions of the pitch- and torque control. The controller is active during the normal power production. If the system switches during the simulation in another mode, like a stop sequence, the external controller is deactivated and the internal controller takes over.

The external controller was written in C++ with Microsoft Visual Studio 2010. The functional range of the controller is explained below. The controller code is attached in the appendix.

3.4.1 Torque control

Below rated generator speed, the rotor speed is regulated by the torque control. The measured generator speed is the input value for the torque control. Via a defined torque-speed table the demanded generator torque is set, see 3.2. Between the defined set points the speed value is interpolated linearly. The torque control is an open loop, shown in figure 3.3.

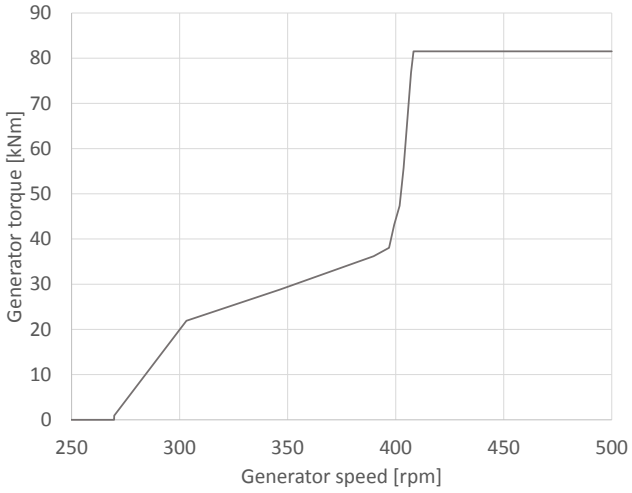

Figure 3.2: Torque-speed table

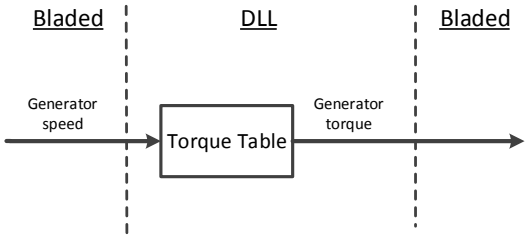

Figure 3.3: Torque control

3.4.2 Pitch control

Above demanded generator speed the generator torque level is constant. To control the rotor speed nevertheless, the blades have to be pitched out of the wind. As shown in figure 3.4 the PD controller is built-up like a closed-loop control.

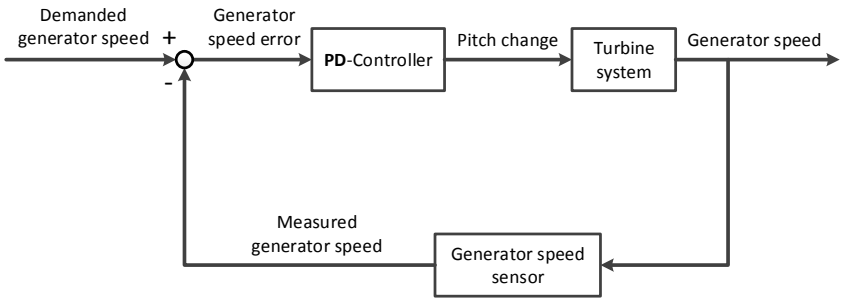

Figure 3.4: Pitch control feedback loop

The rated generator speed is set as the demanded speed value. The spread between demand and measured generator speed is the control error e and is the input value for the PD controller. This controller calculates the pitch change dependent on the error.

The PD controller has a proportional and a derivative part, see figure 3.5. In the proportional term the error is multiplied by the proportional parameter K_p, so that the output value of the P-term is proportional to the current error. In the derivate term the error change over time is determined. Than the rate of change is multiplied by the derivative gain K_d. It should be mentioned that the parameter K_p depends on the pitch angle β: the larger β, the larger the parameter K_p. The values are given in a look-up table. This method is called gain scheduling and is used to give the linear controller a non-linear characteristic [25].

The output values of the two terms are added up to result in the current demanded pitch change. Because of the individual control of the two pitch actuators, the PD Controller is provided twice.

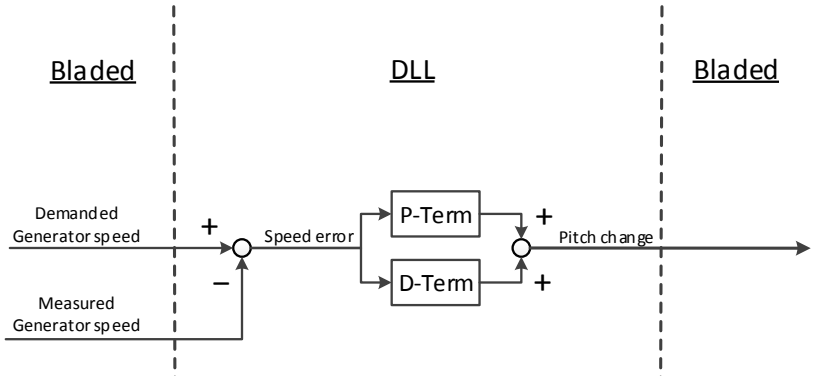

Figure 3.5: PD control

3.4.3 Pitch-teeter control

The pitch-teeter control couples the pitch angle with the teeter angle. Therefore, the measured teeter angle is queried from Bladed and is multiplied with the defined pitch-teeter coefficient. Depending on the blade, the value is added to the pitch change or is substracted from it, see figure 3.6.

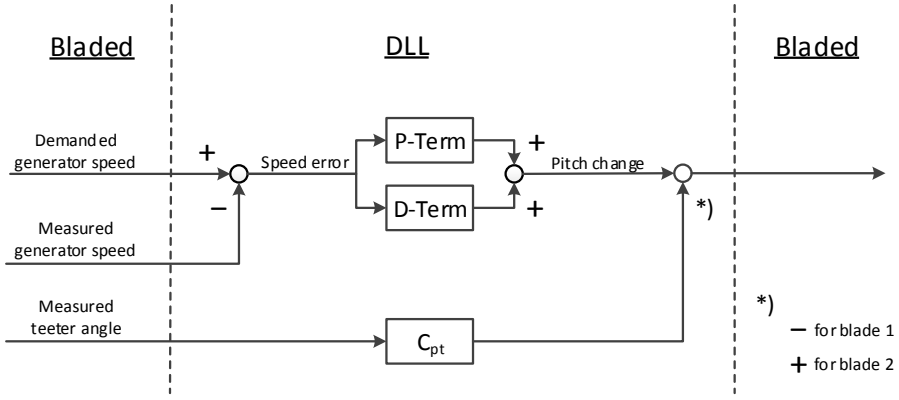

Figure 3.6: Pitch-teeter control

3.5 Validation of the external controller

To validate the performance of the programmed external controller the simulation results are compared to the external controller provided by aerodyn. Because the aerodyn controller doesn't support individual pitch control and therefore pitch-

teeter coupling neither, the pitch-teeter coefficient in the programmed controller was set to 0.

For the validation of the controller dynamics a simple load case was used. An immediate wind speed change of 4 m/s with different initial wind speeds was simulated. The step response of the pitch angle, generator speed and generator torque are shown in figure 3.7.

As a side note it can be observed that the transient effect of the new controller is shorter and has a lower amplitude at the start of the simulation. Thus, the time delay to write the output could be reduced. But this difference was not considered any further. The transient response of the wind speed change is more important to validate the controller.

The pitch actuators respond simultaneously on the wind speed change. The aerodyn controller however has a larger pitch overshoot. But the pitch differences are very small, so that there is almost no disparity between the generator speeds. Approximately eight seconds after the wind speed change, the gradients are almost identical.

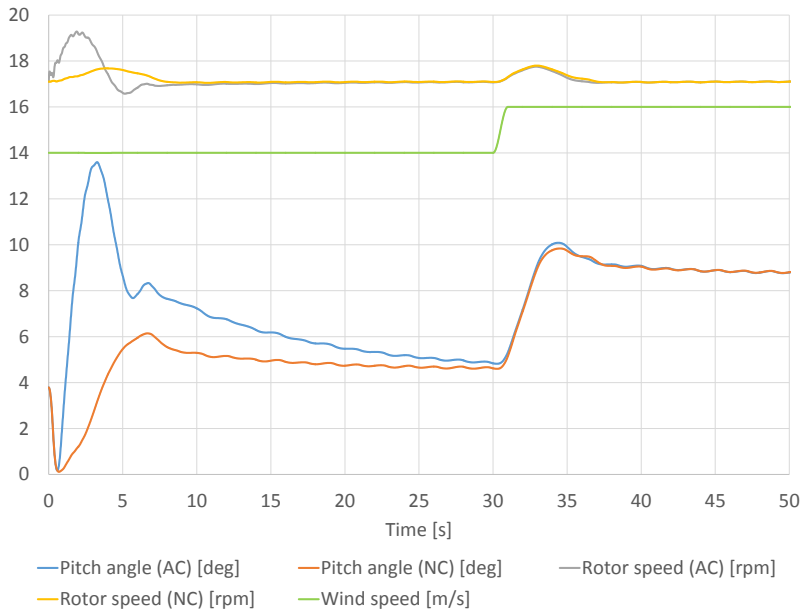

Figure 3.7: Step response

Because this comparison was done without coupling of pitch and teeter movement, it has to be determined in a second step if the pitch-teeter control works correctly, too.

An easy way to show the influence of the pitch-teeter coupling is a simulation below rated wind speed. Because the rated generator speed is not reached in this case, the pitch control outputs a pitch angle of 0 deg. Then the only pitch change is caused by the coupling coefficient of the pitch-teeter control.

In figure 3.8 the pitch-teeter coupling is illustrated for $C_{pt} = 1$ as an example. According to this coefficient, pitch angle and teeter angle have to be equal and this is also shown in the figure. Further results for different coefficients C_{pt} are listed in table 3.4.

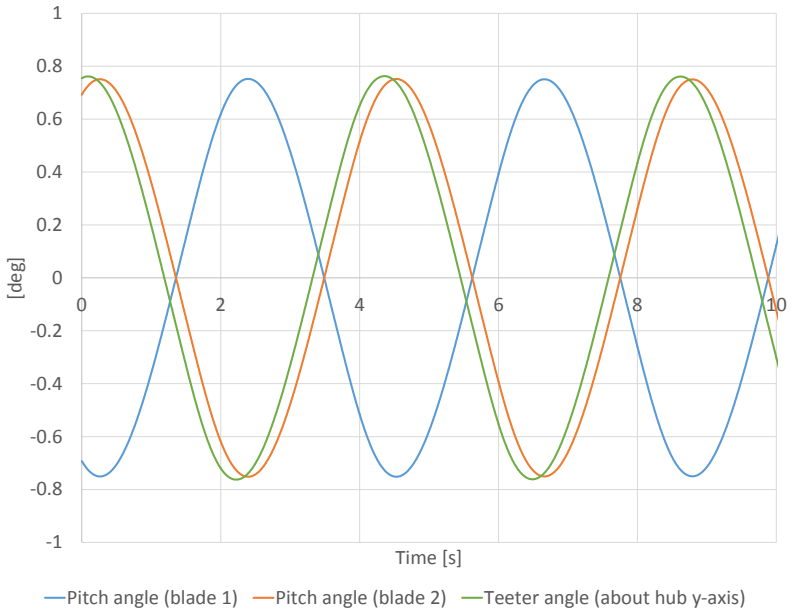

Figure 3.8: Check of the Pitch-teeter control

Table 3.4: Check of the pitch-teeter control

Pitch teeter coefficient	Comparable to delta-3 angle	Measured max. teeter angle ξ_{max} [deg]	Measured max. pitch angle β_{max} [deg]	$\frac{\beta_{max}}{\xi_{max}}$
0	0	0.98	0	0
0.2679	15	0.97	0.26	0.2680
0.5774	30	0.90	0.52	0.5778
1	45	0.76	0.76	1

Chapter 4

Simulation results

4.1 Teeter behavior

In the first simulations the focus is on the teeter motion of the wind turbine. The aim is to check if the influence of the described pitch-teeter couplings is as expected. The calculations thus are performed at steady wind conditions.

4.1.1 Delta-3 coupling

The delta-3 angle was varied from 0 to 75 deg. As expected: the larger the delta-3 angle, the smaller the maximum teeter angle, see figure 4.1.

However, this is not generally valid for large delta-3 angles. A large coefficient between pitch and teeter angle can lead to an unstable teeter motion, especially at higher wind speeds. As shown in figure 4.2 a setting of 75 deg causes a different unstable teeter behavior at a wind speed of 20 m/s.

This phenomenon can be justified with formula (2.7). If the delta-3 angle is increased, the natural frequency of the teetered hub ω_{Teeter} is increased, too. As shown in table 4.1, the teeter natural frequency ω_{Teeter} moves close to the first blade flapwise frequency. Although the values are not exactly the same, it could be assumed that the frequency raise leads to a coupling, which results in resonance. Furthermore, the calculation of the actual Lock number of the rotor blade is complex. The assumed Lock number is rather an approximation than an exact value. Therefore, the actual frequencies ω_{Teeter} may differ a bit.

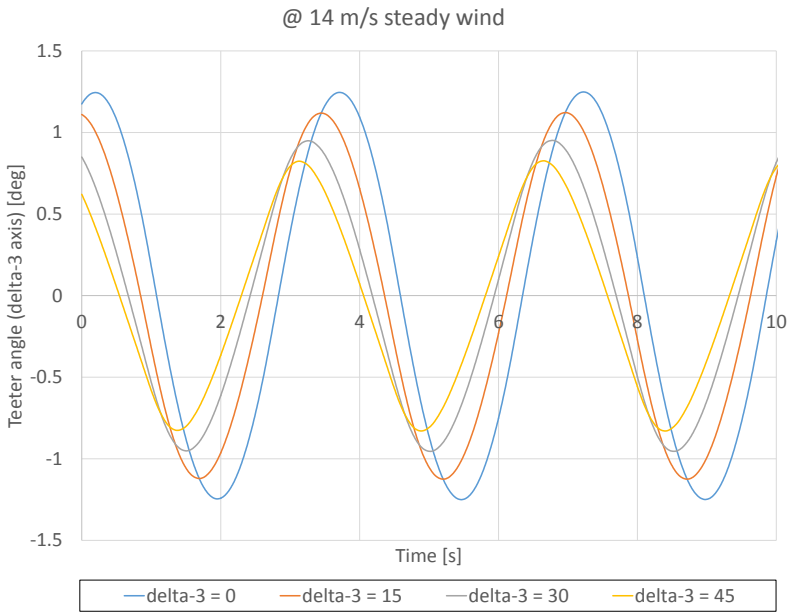

Figure 4.1: Teeter behavior for different delta-3 angle

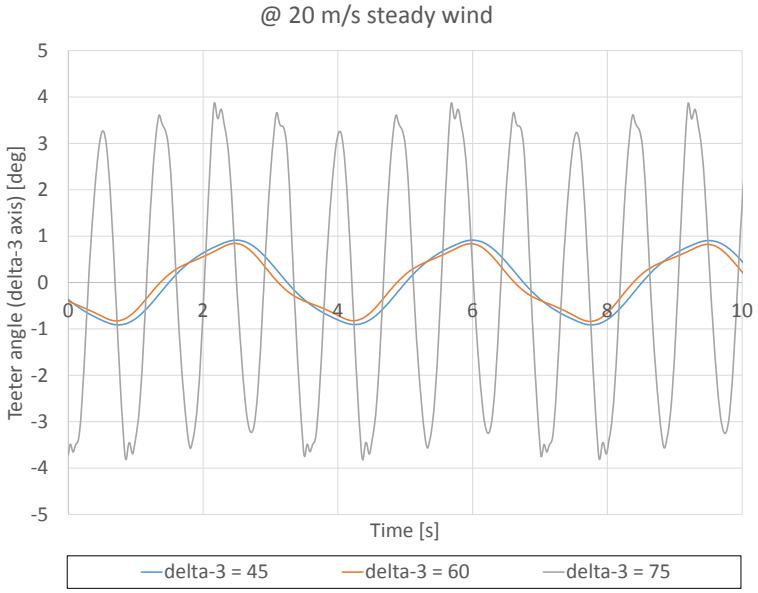

Figure 4.2: Unstable teeter behavior for large delta-3 angle

Table 4.1: Comparison of teeter natural frequency and modal frequencies

Delta-3 angle [deg]	ω_{Teeter}[Hz]
0	0.285
15	0.356
30	0.424
45	0.502
60	0.614
75	0.847

Modal frequencies [Hz]	
Blade 1. flapwise	0.89
Blade 1. edgewise	1.31
Blade 2. flapwise	2.54
Blade 2. edgewise	4.41

4.1.2 Active Pitch-teeter coupling

To allow an easier comparison between delta-3 coupling and active pitch-teeter coupling, the coefficents of the active PTC are usually indicated as the equivalent delta-3 angles in this thesis, although the actual delta-3 angle is 0 for all active PTC. In table 4.2, the delta-3 angles and the equivalent pitch-teeter coefficients C_{pt} are specified.

Table 4.2: δ_3 and the equivalent C_{pt}

δ_3[deg]	C_{pt} [-]
0	0
15	0.268
30	0.577
45	1
60	1.732
75	3.732

The coefficient for the active pitch-teeter coupling has been varied from 0 to 3.732, which is equivalent to 0 to 75 deg. The result is similar to the variation of delta-3 angles. However, an angle of 15 deg leads to a larger teeter amplitude than without pitch-teeter coupling, see figure 4.3. Larger pitch-teeter coefficients have a reducing effect.

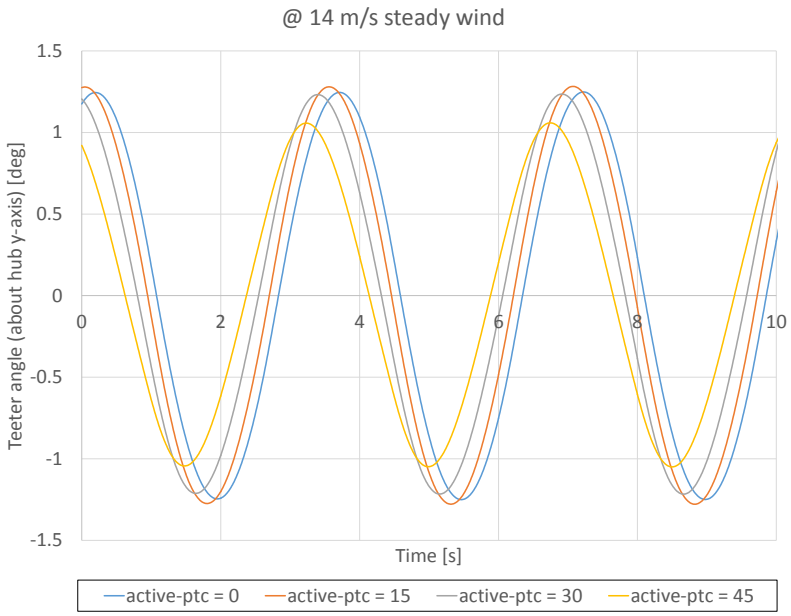

Figure 4.3: Teeter behavior for different pitch-teeter coefficients

Like in section 4.1.1 large coefficients cause irregular large teeter amplitudes as shown in figure 4.4. The effect already appears above 45 deg at a wind speed of 20 m/s. But the resulting teeter motion is not similar to the unstable teeter motion for large delta-3 angle. Therefore, the reason for the instabality is problaly not an increase of the natural teeter frequency but a unsuitable pitch-teeter control.

In figure 4.5, the beginning of a simulation run is shown. While the simulation model with an active PTC of 45 deg reaches stable conditions after about 8 seconds, the pitch and teeter motion of the simulation model with an active PTC of 60 deg remain unstable. An adjustment of the control parameters K_p and K_d could possibly solve this problem.

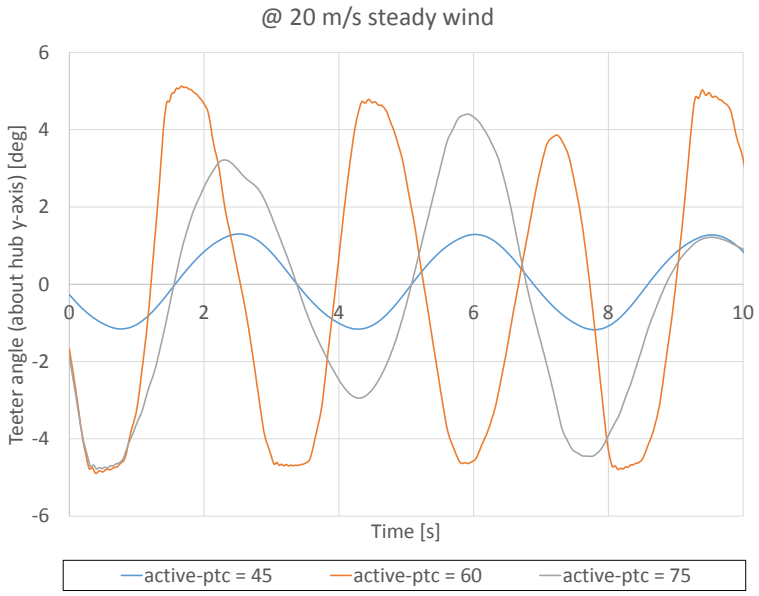

Figure 4.4: Unstable teeter behavior for large pitch-teeter coefficients

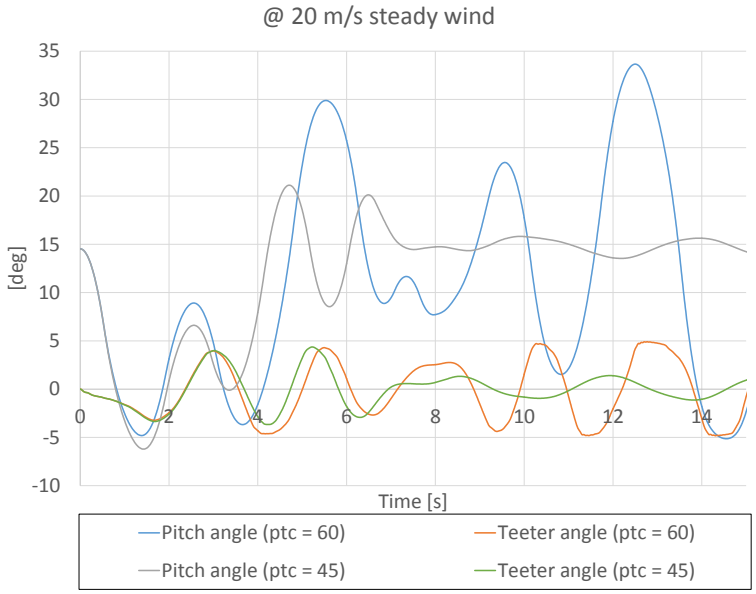

Figure 4.5: Transient response of pitch and teeter motion

4.2 Comparison of pitch-teeter couplings

Comparing the two methods, delta-3 coupling has a larger influence on the teeter motion than the pitch-teeter coefficient. That means the teeter amplitudes of the delta-3 couplings are in every simulated run smaller than the amplitudes of the equivalent active PTC. Figure 4.6 shows a comparison between the coupling methods at a coefficient of $C_{pt} = 1$ ($\delta_3 = 45\,\text{deg}$). It was assumed actually that the teeter amplitudes about the hub y-axis (= aerodynamic teeter axis) will be similar for the two coupling methods. It was also assumed that the teeter amplitude about the delta-3 axis (= mechanical teeter axis) will be larger than the the result for the active PTC. It should also be noted that he difference between the resulting teeter amplitudes rises with the amount of the pitch-teeter coefficient.

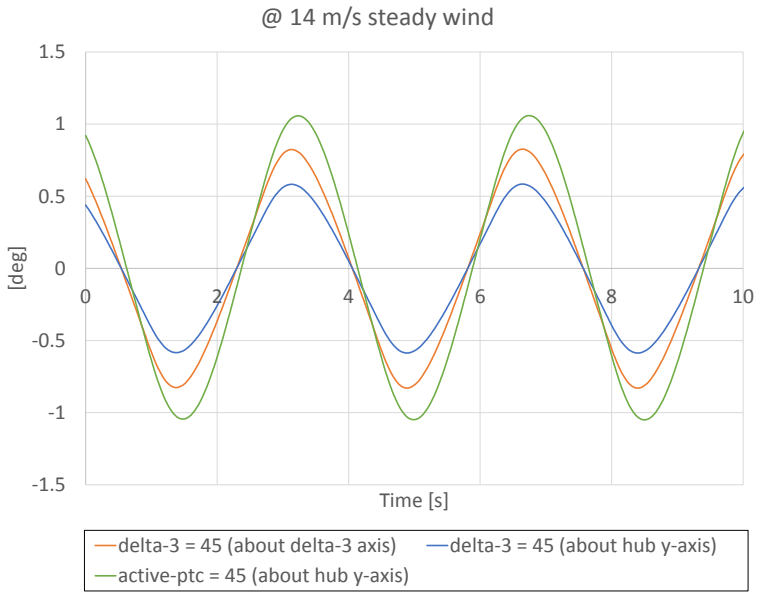

Figure 4.6: Comparison between pitch-teeter couplings

A clear solution of this result could not be found until now. The validation in section 3.5 actually excludes a failure of the external controller. For comparison the teeter movements were also measured in the same coordinate system (around hub y-axis). So a reading error can be excluded, too. Some approaches to explain the difference are listed below.

The inertia of the pitch system

A delta-3 hinge is based on a purely mechanical hinge. Due to the design, the rotor blade is bounded to rotate about the pitch axis. In case of an active pitch-teeter coupling the teeter angle is measured first to calculate the additional pitch change. Therefore, the system has got a delay. The disparity between actual and demanded pitch angle is shown in figure4.7. So the ideal pitch angle can't be set immediately, but a timestep later.

As it can be seen in the diagram, the difference between actual and demanded value is about 0.2 seconds for $C_{pt} = 1$ at a wind speed of 20 m/s. This could have an effect on the teeter motion, but not such a large one to explain the gap between the teeter amplitudes of the coupling concepts.

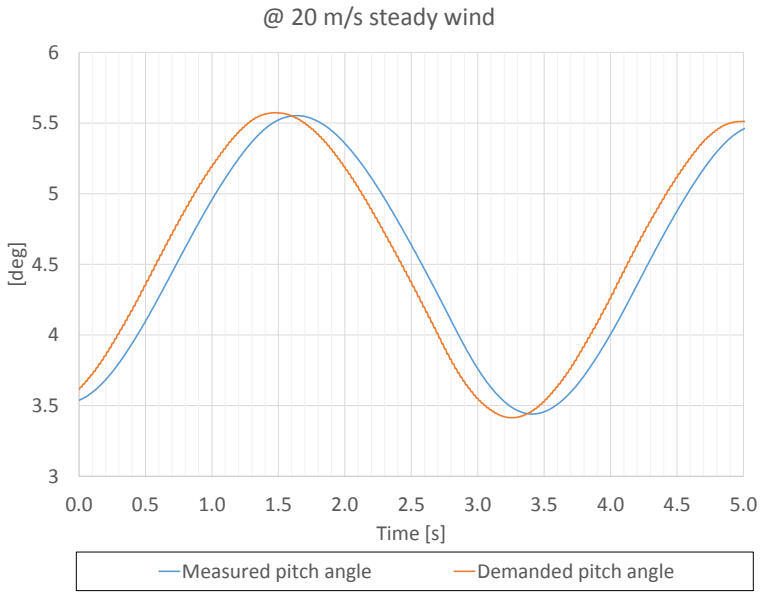

Figure 4.7: Inertia of the pitch system

Simulation model of Bladed

Another possible explanation is a failure in the simulation model of Bladed. Because Bladed is not open sourced, calculation steps can't get checked. Only the basic calculation approaches are listed in the Bladed Theory Manual.

The Bladed support team was also informed about this phenomenon. It has been responded that the underlying model works correctly.

Wrong approach

It is also conceivable that the approaches made in section 2.2.3 are not correct for both methods of pitch-teeter coupling. According to [17], the active PTC has the same effect as a delta-3 angle, if the same coefficient is used.

However, the rotor motion is not exactly the same in both cases caused by the different teeter axis. This can be explained with a simple hypothetical example. Starting in vertical rotor postion, the rotor should teeter 180 deg about the teeter axis. In case of a delta-3 coupling ($\delta_3 = 45\,\text{deg}$) the rotor would reach a horizontal rotor position. As it can be seen in figure 4.8, the rotor rotates in this example 90 deg in rotor rotation direction without a rotation about the shaft axis. A rotor with a mechanical pitch-teeter coupling would not have this additional rotation.

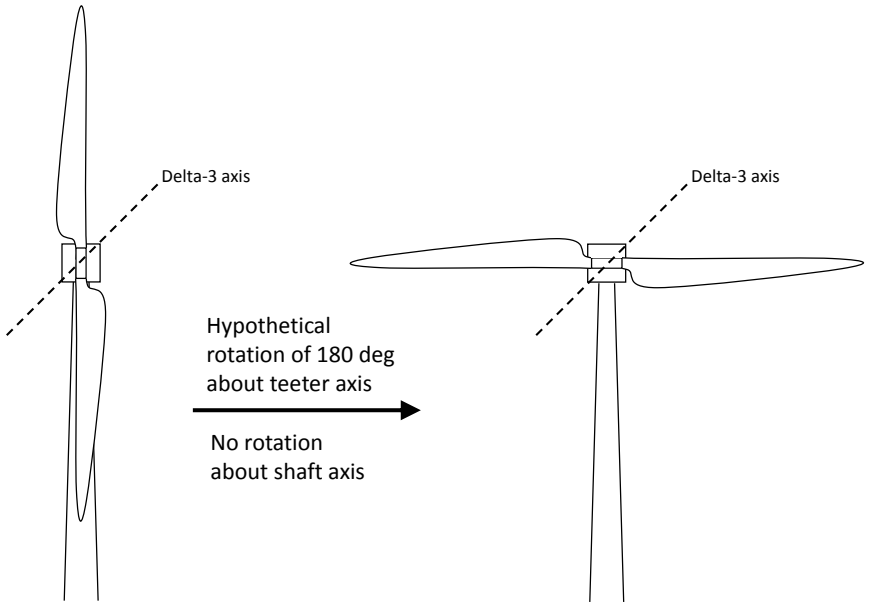

Figure 4.8: Hypothetical teeter angle of 180 deg

These large teeter motions are of course unrealistic but it should explain the fact that the delta-3 rotor teeters also in rotor rotation direction while a rotor with active pitch-teeter coupling only teeters perpandicular to the rotor plane (whatever coefficient C_{pt} is selected).

For small teeter angles the difference of the rotor motions are not very large, but it could have an influence on the aerodynamic damping for example.

However, none of the arguments could be proved so far.

4.3 Parameter study

In this section the following teeter system parameters get analyzed:

- Spring characteristic of the end impact restraint system
- Free teeter angle
- Damping factor of the restraint system
- Delta-3 angle
- Active pitch-teeter coefficient

The basic settings for the restraint system are as described in table 3.3. A delta-3 angle and an active pitch-teeter coefficient of 0 are setted as default, to identify the influence only of the analyzed parameter.

The primary aim in this thesis is reducing the fatigue loads, which is why only the fatigue loads were analyzed in the parameter study.

The differing blade loads caused by wind shear have its most significant effect on the hub My loads. In the following described simulations the main focus is on these loads. The load spectrum over a period of 20 years and the related equivalent loads are evaluated.

4.3.1 Spring characteristic

The basic configuration of the stiffness curve is linear. But also non-linear curves are possible and may bring benefits in relation to the fatigue loads.

Important for a meaningful comparison of different spring characteristics is to ensure that the elastic potential energy up to the maximal permitted teeter angle must not change.

One restraint concept is to use a progressive spring characteristic. The teeter motion is stopped first with lower stiffness, to keep the hub loads low. With increasing teeter angle the spring stiffness also increases. This guarantees the compliance of the potential energy, but increases the hub loads for higher teeter angles, too.

Three different progressive spring characteristics are designed for the parameter study, see table 4.3. The stiffness curve is divided in a soft and a hard stop for the intended progressive characteristic.

Table 4.3: Details of the progressiv spring characteristics

	Teeter range [deg]		Spring rate $\left[\frac{\text{Nm}}{\text{deg}}\right]$		
	From	To	progressiv_1	progressiv_2	progressiv_3
Free teeter	0	3.5	$7.0 \cdot 10^4$	$7.0 \cdot 10^4$	$7.0 \cdot 10^4$
Soft stop	3.5	4.6	$4.33 \cdot 10^7$	$2.51 \cdot 10^6$	$6.86 \cdot 10^5$
Hard stop	4.6	6.0	$1.0 \cdot 10^7$	$1.40 \cdot 10^7$	$1.80 \cdot 10^7$

Another concept is to use a teeter restraint with pre-load. The benefit is higher torque towards the teeter motion right from the first contact with the end stop. Therefore, the first section can be used more efficiently, but the transition to the end stop is not smooth anymore. Again, three different spring characteristics were chosen, see table 4.4. Because Bladed needs a continuous stiffness curve, the transition between free teeter and end impact section is a high increase and not a stiffness jump. The pre-loaded stiffness is available 0.1 deg after end stop contact.

Table 4.4: Details of the pre-load spring characteristics

	Teeter range [deg]		Spring rate $\left[\frac{\text{Nm}}{\text{deg}}\right]$		
	From	To	pre-load_1	pre-load_2	pre-load_3
Free teeter	0	3.5	$7.0 \cdot 10^4$	$7.0 \cdot 10^4$	$7.0 \cdot 10^4$
Pre-load	3.5	3.6	$2.25 \cdot 10^7$	$4.75 \cdot 10^7$	$7.26 \cdot 10^7$
Stop	3.6	6.0	$4.71 \cdot 10^6$	$2.58 \cdot 10^6$	$4.57 \cdot 10^5$

The researched spring characteristics of the end stop are shown in figure 4.9. The diagram starts at the beginning of the end stop (3.5 deg). The free teeter section with the low spring rate is not illustrated due to the clarity of the diagram.

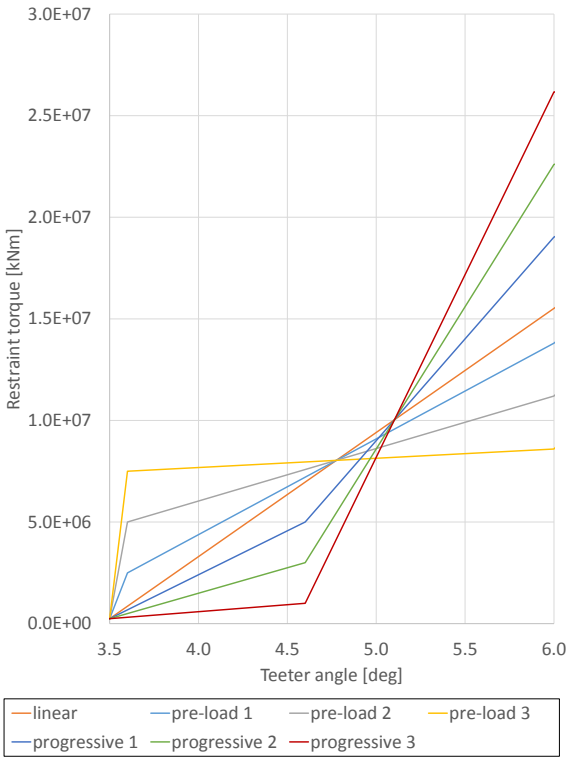

Figure 4.9: Variation of the spring characteristic

The simulation results are illustrated in figure 4.10. It is shown that the higher the maximal teeter restraint, the higher the maximal loads.

So a pre-stressed end stop can reduce the maximal fatigue loads of a teetered hub. But the number of low level operating loads increases at the same time due to the pre-load and the related high restraint for smaller teeter angle.

The effect of a progressive spring characteristic is reverse. Number and level of the operating loads decrease, the extreme loads increase.

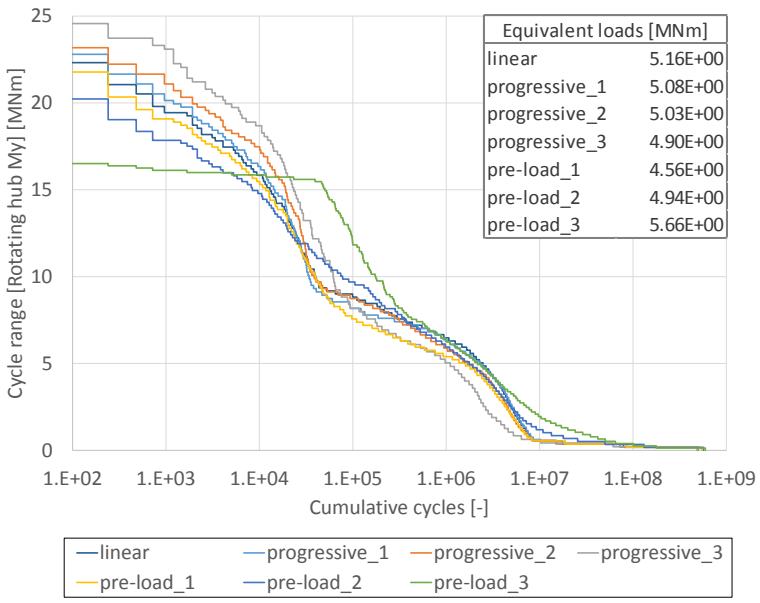

Figure 4.10: Load spectrum Hub My - variation of spring characteristic

The results can be rated by comparing the damage equivalent loads. According to it, a progressive as well as a pre-stressed teeter restraint can reduce the fatigue loads in comparison to the basic linear spring characteristic. But a low pre-load has the most positive effect, according to the equivalent loads.

However, a too high pre-load influences the fatigue loads negatively. As mentioned, the number of low level operating loads increases because of the high restraint torque at the beginning of the end stop. Furthermore, the end stop impact can be so strong that the rotor is set into vibration. These vibrations are additional amplitudes, which affect the load spectrum negatively. The impact in the stiff end stop is shown in figure 4.11 for configuration pre-load_2.

This phenomenon always occurs, when the spring stiffness is high and the transition to this stiffness is not smooth enough.

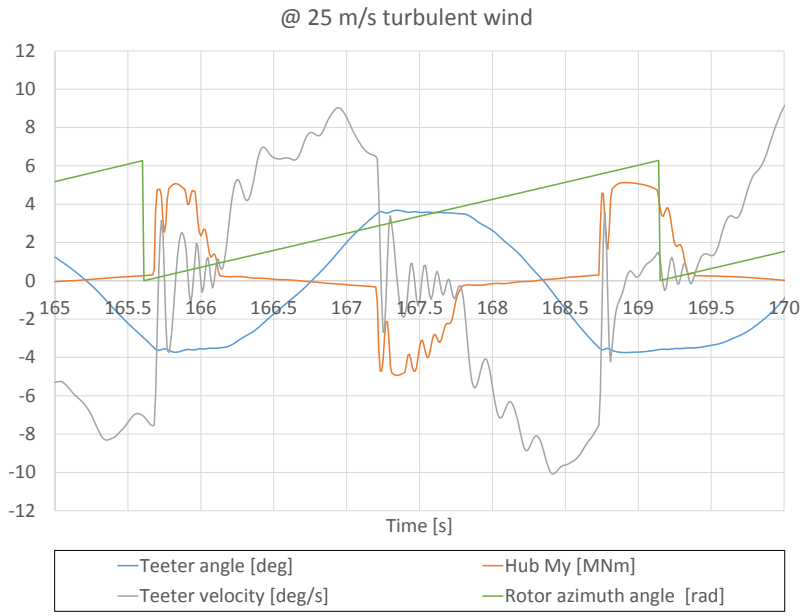

Figure 4.11: End stop impact with large spring ratio

4.3.2 Free teeter angle

The choice of the free teeter angle must always be a compromise. On the one hand, a large angle range without restraint reduce the hub My loads. On the other hand, the teeter motion has to be limited to prevent a contact of rotor blade and turbine tower and to reduce the complexity of the wind turbine design.

In this section the free teeter angle is varied. The spring characteristic is always linear. Like in the section before, the requirement for the angle variation is that the potential energy remains constant to the basic setting. This means if the free teeter angle is raised, the spring stiffness has to be increased.

The different variations are listed in table 4.5. The resulting teeter restraints are shown in figure 4.12.

Table 4.5: Variation of the free teeter angle

	Free teeter			End stop		
	From	To	Spring rate	From	To	Spring rate
	[deg]		$\left[\frac{\text{Nm}}{\text{deg}}\right]$	[deg]		$\left[\frac{\text{Nm}}{\text{deg}}\right]$
fta_0.1	0.0	0.1	$7.0 \cdot 10^4$	0.1	6.0	$1.15 \cdot 10^6$
fta_2.5	0.0	2.5	$7.0 \cdot 10^4$	2.5	6.0	$3.16 \cdot 10^6$
fta_3.0	0.0	3.0	$7.0 \cdot 10^4$	3.0	6.0	$4.26 \cdot 10^6$
fta_3.5	0.0	3.5	$7.0 \cdot 10^4$	3.5	6.0	$6.11 \cdot 10^6$
fta_4.0	0.0	4.0	$7.0 \cdot 10^4$	4.0	6.0	$9.51 \cdot 10^6$
fta_4.5	0.0	4.5	$7.0 \cdot 10^4$	4.5	6.0	$1.68 \cdot 10^7$

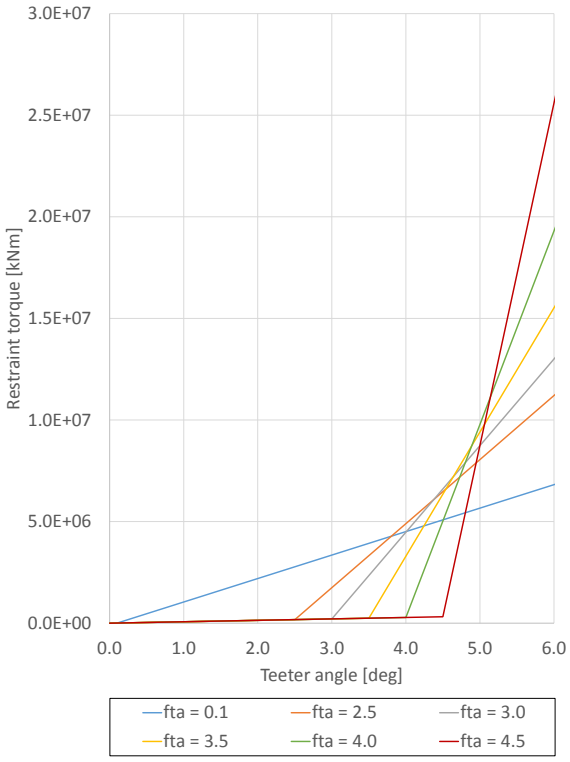

Figure 4.12: Variation of the free teeter angle

When the free teeter range is expanded, less teeter amplitudes reaches the end stop. Therefore the number of operating loads decreases, as shown in figure 4.13. However, when the rotor contacts the end stop, the loads are higher than for the basic model caused by the larger stiffness. Like in chapter 4.3.1, a large restraint torque causes large extreme loads.

The opposite effect is shown, when the free teeter angle is decreased. The number of operating loads increases and the extreme loads are reduced. This effect becomes particularly apparent by looking at the example with almost no free teetering (= 0.1 deg).

The calculation of the equivalent loads indicates that an increase of the free teeter angle can reduce the fatigue loads. A reduction of the free teeter range cannot reduce the results. The higher number of load amplitudes cannot be compensated by smaller extreme loads.

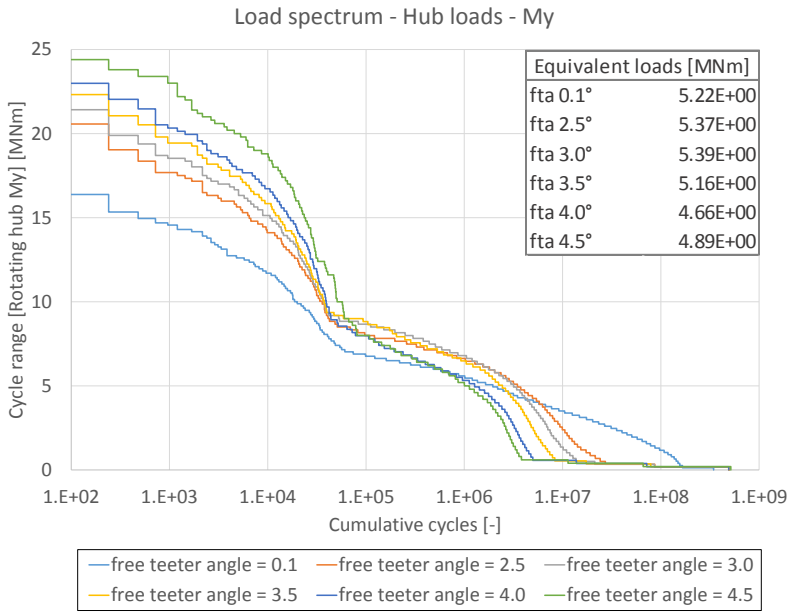

Figure 4.13: Hub My load spectrum - variation of free teeter angle

Nevertheless, the equivalent load of restraint model fta_4.5 is larger than the result of model fta_4.0. So it seems that a larger free teeter range not always reduce the fatigue loads. This can be explained by the large stiffness jump during the contact with the end stop. The impact can be so strong that the rotor is set into vibration, as already mentioned in section 4.3.1.

4.3.3 Teeter damping

In the previous simulations a damping factor was considered caused by teeter bearing friction. The end stop was assumed as a spring.

In this chapter, the end stop is a spring-damper element. In order to enable the spring-damper system, the considered bearing friction has to be deactivated because Bladed only allows one linear damping coefficient in the restraint system. There is no dampening effect in the free teetering section, aerodynamic damping excluded.

The variations of the damper element of the end stop is shown in table 4.6.

Table 4.6: Variation of the damping factor

	Damping ratio D_{stop}	corresponds to damping constant c_h
	[-]	[Nms]
D_0.04	0.04	$1.57 \cdot 10^7$
D_0.08	0.08	$3.13 \cdot 10^7$
D_0.16	0.16	$6.27 \cdot 10^7$
D_0.32	0.32	$1.25 \cdot 10^8$

The fatigue loads of the analysis are shown in figure 4.14. The configuration D_0.32 is not illustrated because the resulting fatigue loads are much higher in comparison to the other results. Nonetheless, the equivalent load is given.

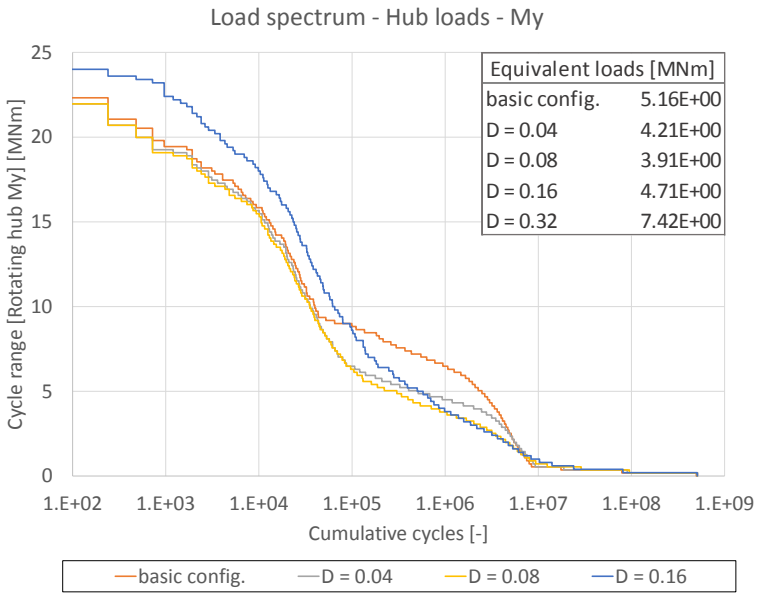

Figure 4.14: Hub My load spectrum - variation of damping factor

The load spectrum illustrates that an additional end stop damper can reduce the hub loads. The best result is obtained by $D_{stop} = 0.08$. A higher damping ratio causes higher loads again. The rise is caused by the general characteristics of a damper.

Unlike the spring stiffness, which is dependent on the spring displacement, the damper force is related to the velocity. So the restraint due to the end stop damper is largest at the time of first contact. After the rotor reaches the end stop the teeter velocity decreases and so the damping force. So if the damping constant is too large, high load peaks can occur, illustrated in the time series in figure 4.15.

The figure shows one rotor revolution. When the teeter angle reaches the end impact (= 3.5 deg), the teeter velocity decreases and the restraint increases abruptly. At maximal teeter amplitude the damping force is 0 because the rotor does not move. Only the spring load acts on the hub in this moment.

A second disadvantage is also shown in figure 4.15. The damping element operates in the backward motion, too. For that reason, the hub My load became negative. If the rotor left the end stop section, the damper influence ends abruptly, which causes oscillations in the teeter velocity. The higher the damping constant, the higher the described effect.

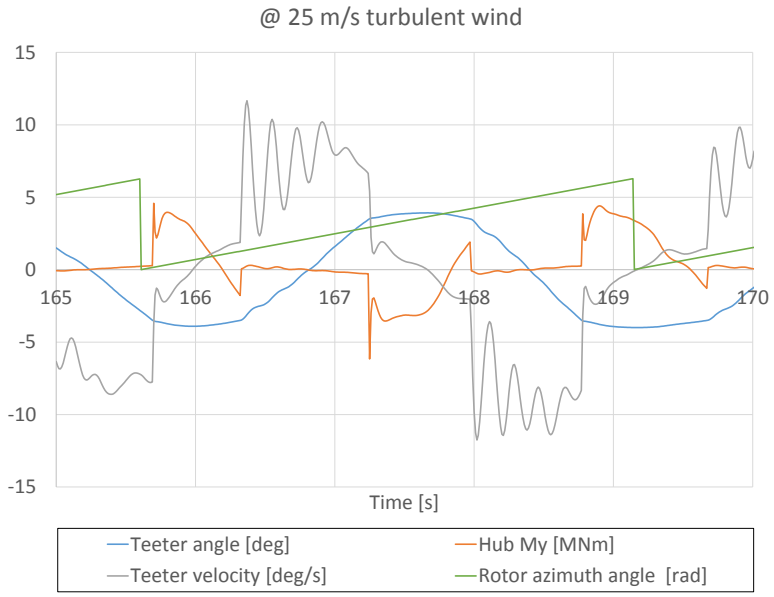

Figure 4.15: End stop impact with high damping ratio

4.3.4 Delta-3 angle

The influence on the fatigue loads was analyzed by a variation of the delta-3 angle from 0 deg to 60 deg in steps of 15 deg. Because of the oscillation problems for a delta-3 angle of 75 deg, this set was not considered in the simulation. The obtained hub loads would be much higher caused by the high end stop impact loads.

The result is shown in figure 4.16. As shown in section 4.1.1, the teeter amplitude can be reduced by an increasing delta-3 angle. This also leads to a reduced number of end stop impacts. Therefore, the hub loads decreases with increased delta-3 angle. The equivalent loads are less for a delta-3 angle of 60 deg and are reduced by about 57 %.

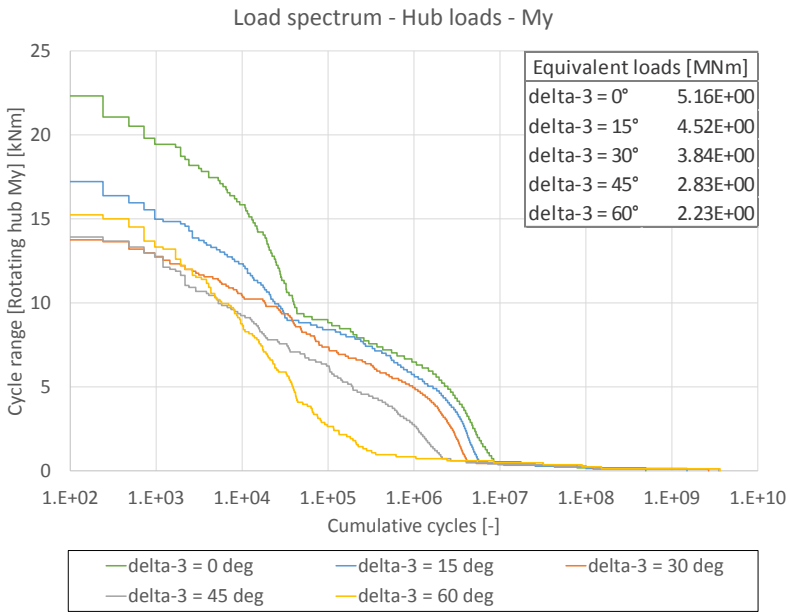

Figure 4.16: Hub My load spectrum - variation of delta-3 angle

4.3.5 Active pitch-teeter coefficient

Because of the unstable teeter motion for an active pitch-teeter coefficient of 60 deg and 75 deg, the coefficient was only be varieted from 0 to 1, which corresponds to delta-3 angles of 0 deg to 45 deg.

It was already discussed that the effect of an active pitch-teeter coupling is similar to a delta-3 axis, but with a lower influence despite the same pitch-teeter coefficient. Therefore, the hub loads can not be reduced like in case of a delta-3 axis. Again, the best result was given by the largest coefficient ($C_{pt} = 1$), which reduces the hub loads by about 6 % in comparison to a configuration without PTC coefficient.

A second reason for the lower influence on the fatigue loads in comparison to the delta-3 coupling is the fact that the active pitch-teeter coupling does not operate when the wind turbine is parked. Because all load cases are simulated without a teeter lock the rotor can also teeter in parked mode (DLC 6.4). While the delta-3 coupling can influence the teeter motion, the active PTC is deactivated.

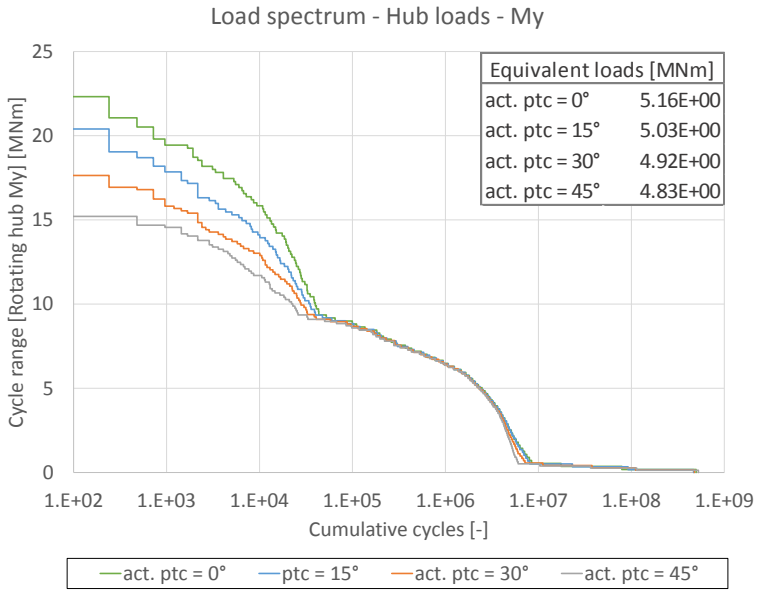

Figure 4.17: Hub My load spectrum - variation of active pitch-teeter coefficient

4.4 Comparison of the results

In figure 4.18 the influence on the damage equivalent loads are compared. It is shown that a delta-3 coupling has the largest potential of all analyzed parameters. The hub My fatigue loads could be reduced by 57 %. If the teeter oscillation problems would not appear, a larger delta-3 angle than 60 deg would reduce the out-of-plane bending moments further.

This is also the case for the active pitch-teeter coupling. If the pitch-teeter control would be optimized for high coefficients, the fatigue loads could be reduced further. However, the influence on the fatigue loads is low for all analyzed pitch-teeter coefficients. The maximal improvement is 6 %.

Also an end stop damping could have a large effect. The fatigue loads could be reduced by 24 % with an additional damping ratio of $D = 0.08$ in comparison to the basic configuration of the end stop teeter system.

The variation of the free teeter angle has shown that a teeter angle reduction has no positive effect on the fatigue loads. But a expansion to a larger free teeter range could reduce the loads by up to 10 %.

The analysis of the different end stop spring characteristics has shown that a

progressive as well as a pre-loaded spring leads to lower fatigue loads than a linear spring rate. The largest improvement is provided by a small pre-load. The fatigue loads could be reduced by 12 %.

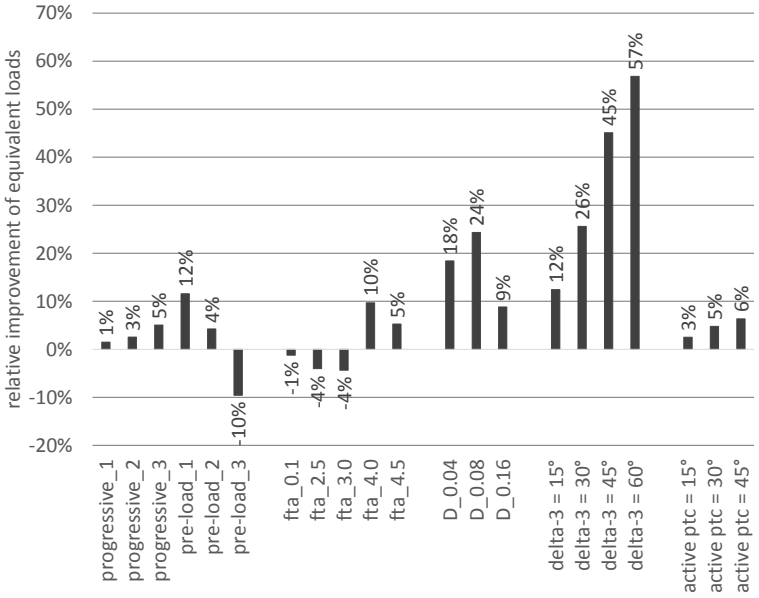

Figure 4.18: Comparison of the damage equivalent loads

4.5 Influence of a teeter lock

As already mentioned, a disadvantage of an active PTC is the fact that it does not operate in parked mode. The pitch control is deactivated while the pitch angle is set to 90 deg, whereas a delta-3 coupling operates also in parked conditions. This difference increases the deviation of the fatigue load results.

The loads, which occur during the parked situations, could be minimized by locking the degree of freedom around the teeter axis. The influence of this teeter lock is shown in figure 4.19. A delta-3 coupling and an active PTC with $C_{pt} = 1$ are compared. Only the parked situations are covered by the teeter lock.

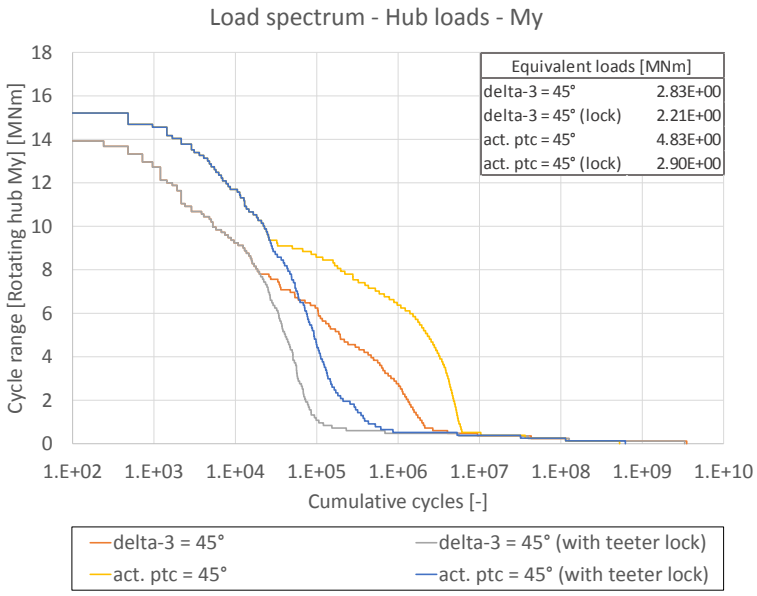

Figure 4.19: Influence of a teeter lock on the fatigue loads

It is shown that the teeter lock can not reduce the high loads in the spectrum. The teeter motion during parked situation leads instead to a high number of smaller loads, which have a large influence on the fatigue. Therefore, the teeter lock decreases the fatigue loads significantly, especially in case of the active PTC. The fatigue loads could be reduced by about 40 % in this example only by locking the teeter motion in the parked load cases.

4.6 Finding an optimum

It seems reasonable to combine the best results of the parameter analysis, to get a further reduction of fatigue loads. However, it is not useful, because the parameters influence each other, which might result instead in higher hub loads.

If the free teeter angle gets changed, for example, the spring characteristic of the end stop changes as well. A pre-loaded spring, which was defined in the parameter analysis, would now have a different influence on the hub loads. Another example is the influence of the delta-3 axis to the maximal teeter amplitude. If the teeter motion gets reduced due to the pitch-teeter coupling, the teeter restraint system could be designed in a smaller teeter range.

Another problem finding an ideal optimum is the fact that every possible combination of parameter variation have to be simulated and analyzed. This leads to $6 \cdot 5 \cdot 3 \cdot 4 \cdot 3 = 1080$ additional simulations. There are also some optimisation methods that could find the optimum with a reduced number of simulations, like the design of experiments (DOE). These methods require to set up a more complex mathematical model, which could not be considered in the scope of this thesis [4].

The optimum will instead be estimated only with the knowledge of the parameter analysis. Furthermore, the teeter restraint system should also be optimized in order to reduce extreme loads, too, even if they are not analyzed in this thesis.

The extreme hub loads depends on maximal restraint torque of the teeter end stop. This could be reduced by enlarging the end stop section. The spring ratio and the maximal restraint thus are lowered.

By increasing the end stop range the free teeter angle decreases. It was shown in figure 4.13 that this leads to a rise of the fatigue loads caused by a higher number of end stop impacts. But if one choose a high delta-3 angle, the teeter amplitude is reduced, which would equalize the effect.

This strategy results in following teeter system parameters:

- free teeter angle of 2.5 deg
- linear spring ratio of 3159 $\frac{\text{kNm}}{\text{deg}}$
- damping caused by teeter friction (no end stop damping)
- delta-3 angle of 60 deg

A additional damping is not considered despite the positive influence on the fatigue loads. It was observed that the delta-3 coupling is negatively affected by an end stop damping. Further researches were not done to solve this problem.

In the following, the results of the optimized model are compared to the simulation model with a rigid hub. The simulations also include a optimized model with a teeter lock for the parked load cases. In addition to the hub My fatigue loads, the results for the Mx, Mz and Fx loads are presented, too.

The hub My fatigue loads are shown in figure 4.20. The optimized configuration leads to significantly better results. For that reason, the damage equivalent loads can be reduced by 72 %. The additional teeter lock has only a low additional influence on the loads.

The analysis of the hub Fx and hub Mx loads show only a very small improvement in comparison to the rigid hub. The teeter lock has no influence on the loads.

In contrast, the hub Mz fatigue loads are increased for the optimized teetering rotor by 17 %. The high loads in the load spectrum of the rigid hub, however, could not be retraced. In any of the fatigue load cases occur such a large load amplitude. So it is assumed that the maximal load step is caused by a simulation error, which would increase the difference between the equivalent loads even further.

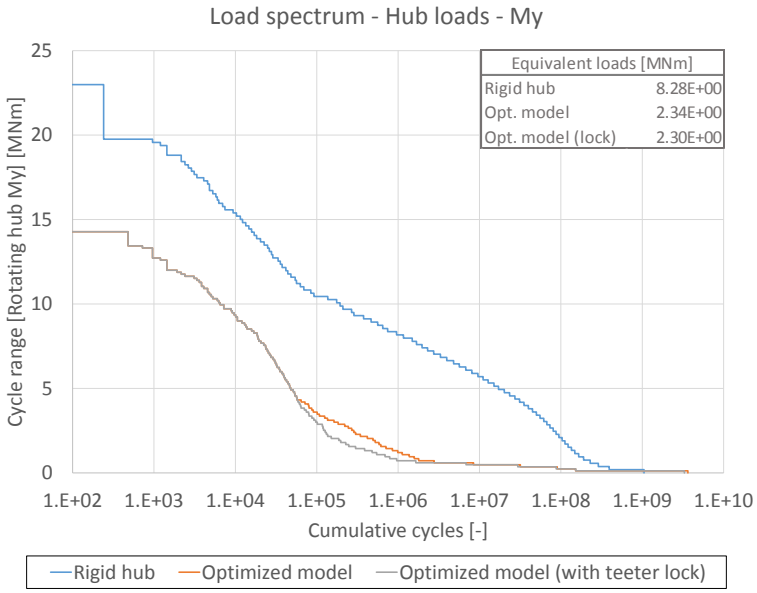

Figure 4.20: Hub My load spectrum of rigid and optimized teetering hub

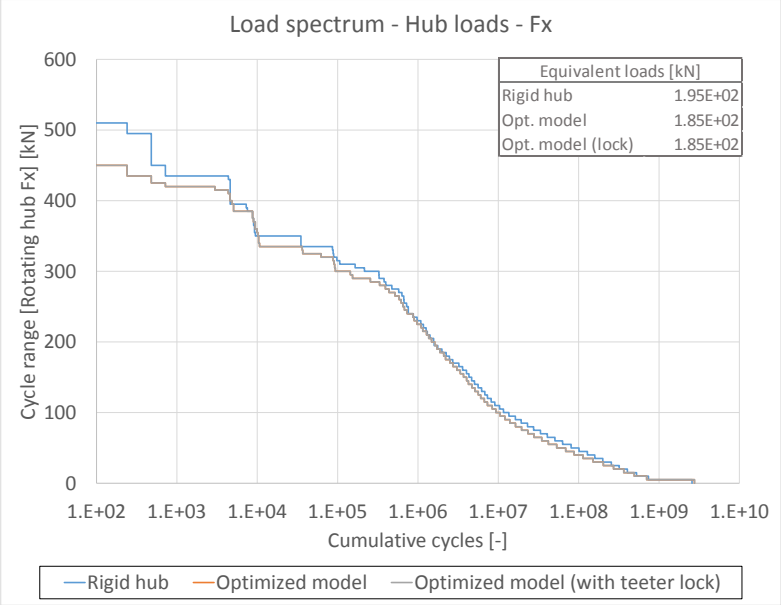

Figure 4.21: Hub Fx load spectrum of rigid- and optimized teetering hub

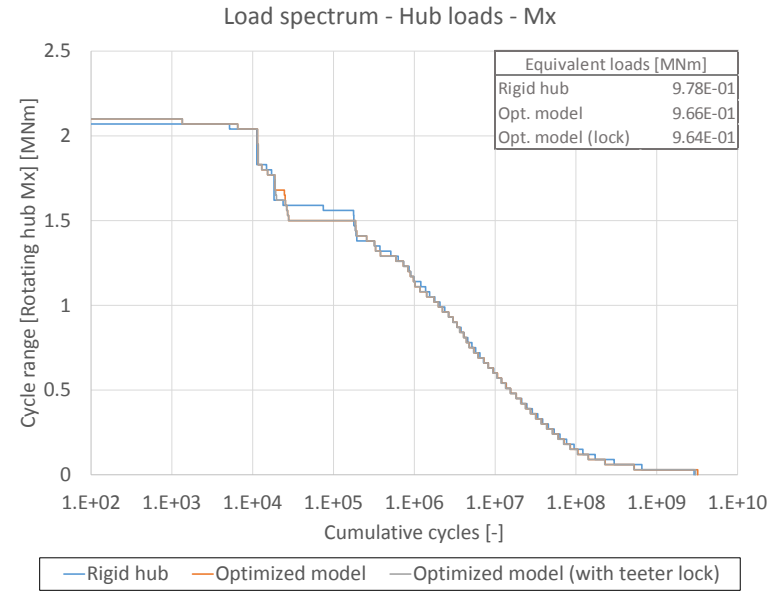

Figure 4.22: Hub Mx load spectrum of rigid and optimized teetering hub

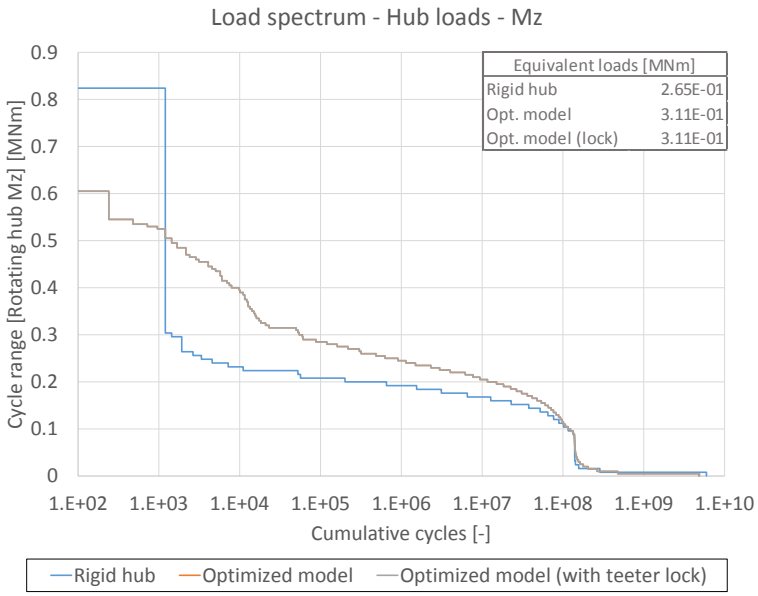

Figure 4.23: Hub Mz load spectrum of rigid and optimized teetering hub

Chapter 5

Conclusion

5.1 Conclusion of the results

External controller

A new external controller has been developed in this thesis. The aim was to achieve a control characteristic similar to the previous controller, but with an additional active pitch-teeter coupling.

A comparison between the controllers has shown that the pitch behavior is similar. A step response to a change in wind speed produced a smaller pitch overshoot for the new developed controller, which results in a slower restoring of the rated generator speed. So the new controller is a bit more damped than the previous one, but the differences are small and have therefore no influence on the evalutations of the hub loads.

To verify the active pitch-teeter coupling, the teeter angle and the pitch angle were compared at a wind speed below rated. The pitch control of the power control is then deactivated and the pitch is only influenced by the active pitch-teeter coupling. The results have shown that the pitch-teeter coupling works as required. For that reason, the external controller could be integrated in the simulation model and could be used for the simulations.

Teeter behavior

To analyze the influence of the pitch-teeter coupling on the teeter amplitude, different delta-3 angles and pitch-teeter coefficients, respectivily, have been compared

to each other. The results have shown that an increasing of the pitch-teeter coefficient leads to a decreasing teeter amplitude, as expected.

However, high pitch-teeter coefficients can lead to an unstable teeter behavior, whether for delta-3 or active pitch-teeter coupling. In case of the delta-3 coupling, the effect could be explained with an increase of the natural teeter frequency ω_{Teeter}. The frequency moves close to the first blade flapwise frequency, which leads to a frequency coupling and the described unstable teeter motion. Because the parameters of the simulation model were assumed from the SCD3.0-100 and were not modified for the teetering hub, it should be possible to solve these resonance problems. The teeter frequency ω_{Teeter} as well as the modal frequencies depend on the blade mass of inertia, for example. The teeter frequency is also influenced by the rotor speed. If these parameters were adjusted, a stable teeter behavior should also be possible for very large delta-3 angles.

In case of stability of the active pitch-teeter control, it was assumed that the pitch control parameters are not appropriate for such high C_{pt}. The parameters K_p and K_d are adjusted and validated for a teetering hub without PTC. Due to the additional coupling, other parameter values are needed.

It was shown for both coupling methods that the teeter amplitude could be decreased and it was expected that the results for a specific delta-3 angle and the equivalent coefficient for the active coupling will be similar. But the results have shown that the active coupling has a much less effect on the teeter amplitude. Different possible explanations have been discussed but a conclusive answer to the described phenomenon could not be found.

Parameter study

The parameter study has shown that a delta-3 coupling has the largest potential to reduce the fatigue loads. Without the frequency coupling at high delta-3 angles the fatigue loads would probably be reduced even further.

The influences on the fatigue loads for the other parameters are significantly smaller. This is because this parameters are part of the end stop characteristic, except the active pitch-teeter coupling. So they can only affect the teeter motion, when the rotor has already reached the end stop. The delta-3 coupling, in contrast, acts on the whole teeter range and can therefore reduce the number of end stop impacts and not only the restraint torque of the end stop.

But because a end stop is definitely needed for a teetering rotor, it is gratifying to see that improvements could be achieved in every parameter variation.

Overall

Overall, the simulation results revealed the large potential of a pitch-teeter coupling to reduce the teeter amplitude and therefore the fatigue loads. Also the teeter end stop parameters could be modified in order to reduce the operational loads.

The out-of-plane hub bending moments are one of the crucial loads, which influence the design of the turbine components. In comparison to a rigid hub, the fatigue loads of these out-of-plane bending moments could be reduced by 72 % with the opimized teeter system.

5.2 Outlook

Further researches

The researches were done with a focus on the fatigue loads. But these loads are only the half of the design consideration. The other half is the analysis of the extreme loads. For that purpose, extreme wind conditions and possible turbine system faults have to be analyzed. It has been observed in [14] that a teetering hub causes higher extreme loads than a turbine with rigid hub. However, the underlying teeter end stop system was not adjusted sufficiently. Compared to [14], the results for the extreme loads should be improved.

The teeter lock should be another research focus. It was already mentioned that all load cases were simulated without a teeter lock, except for the optimized model. Therefore, the rotor also teeters uncontrollably in parked conditions. A turbine designer would probably use a teeter lock to prevent a teeter motion at least for this parked mode. It is also possible to lock the teetering in situations of low rotor speed, because the restoring forces of the teeter motion are then decreased.

It was mentioned that two-bladed turbines are suitable especially for offshore installations. Further researches should therefore consider offshore turbines and offshore conditions like the sea state. A simulation of a teetering rotor, which is affected by the additional motion of a floating platform, is particularly interesting.

Further development of the external controller

The external controller was developed in this thesis to enable the pitch and torque control and also the active pitch-teeter coupling. It is a good basis for further developments. The individual pitch control which is already used to couple the

pitch and teeter motion could be expanded for cyclic loads caused by tower shadow, for example. To reduce the loads, the blade is pitched in front of the tower. The rotor position is needed therefor as an additional controller input value.

Theoretically, it is also possible to couple the pitch signal directly with the blade loads. The aim would be to pitch the blades in order to reach equal loads at both blades. As a result the blade loads would cancel each other out in the hub. The resulting hub loads would be nearly 0, theoretically.

Therefore, a further interesting research step would be to compare the fatigue load results of a teetering hub with a rigid hub and an additional individual pitch control, as described.

Appendix A

External controller code

```
1  #pragma comment(lib, "ExternalControllerApi.lib")
2
3  #include "ExternalControllerApi.h"
4
5  using namespace GHTurbineInterface;
6
7
8  // --- INITIALISIERUNG ---
9
10 double ci; // Communication Interval
11 double e_pitch = 0; // Regelabweichung Pitch
12 double e_pitch_alt = 0; // Regelabweichung Pitch in
       vorheriger Schleife
13 double gspeed_rated = 42.7497; // Nenndrehzahl Generator
14 double torque_rated; // Drehmoment ermittelt aus der Torque
      -Table (Sollwert)
15 double gspeed_measured; // gemessene Generatordrehzahl
16 double torque_measured; // gemessenes Drehmoment
17 double pitch1_measured; // gemessener Pitch-Winkel (Blatt1)
18 double pitch2_measured; // gemessener Pitch-Winkel (Blatt2)
19 double kp_pitch = 0.016; // Verstärkungsfaktor des P-
       Reglers (Pitch)
20 double kd_pitch = 0.00048; // Verstärkungsfaktor des D-
       Reglers (Pitch)
21 double torque_demand; // berechnetes Drehmoment - Uebergabe
```

```
    an Bladed
22 double torque_demand_alt = 81520;
23 double torque_diff;
24 double pitch_demand1; // berechneter Pitch-Winkel (Blatt1)
    - Uebergabe an Bladed
25 double pitch_demand2; // berechneter Pitch-Winkel (Blatt2)
    - Uebergabe an Bladed
26 double pitch_demand1_alt = 0; // berechneter Pitchwinkel (
    Blatt1) in vorheriger Schleife
27 double pitch_demand2_alt = 0; // berechneter Pitchwinkel (
    Blatt2) in vorheriger Schleife
28 double tt_n[13] = {0, 28.2324, 28.2481, 31.7478, 36.2833,
    40.8187, 41.5653, 41.8156, 42.0774, 42.2711, 42.6345,
    42.7497, 52.3598}; // Torque-Table (Generatordrehzahl)
29 double tt_m[13] = {0, 0, 920, 21910, 28820, 36200, 38050,
    43190, 47360, 55730, 76840, 81520, 81520}; // Torque-
    Table (Generatormoment)
30 double gain_angle[5] = {0, 0.0873, 0.244, 0.436, 1.75};
31 double gain_factor[5] = {1, 1, 1.5, 2, 2};
32 double gain1_kp;
33 double gain2_kp;
34 double a_interpol; // Variable für Interpolation
35 double b_interpol; // Variable für Interpolation
36 double c_interpol; // Variable für Interpolation
37 double teeter_angle;
38 double pitch_teeter1;
39 double pitch_teeter2;
40 double ppk = 1;
41
42
43 // --- CONTROLLER-SCHLEIFE ---
44
45 extern "C"
46 {       int __declspec( dllexport ) __cdecl CONTROLLER (
    const turbine scd)
47         {
48
49
50                 // --- WERTUEBERGABE VON BLADED ---
```

```
51
52                  gspeed_measured = GetMeasuredGeneratorSpeed
                        (scd);
53                  torque_measured =
                        GetMeasuredGeneratorTorque(scd);
54                  pitch1_measured = GetMeasuredPitchAngle(scd
                        ,0);
55                  pitch2_measured = GetMeasuredPitchAngle(scd
                        ,1);
56                  teeter_angle = GetMeasuredTeeterAngle(scd);
57                  ci = GetCommunicationInterval(scd);
58
59
60                  // --- TORQUE-TABLE-ABFRAGE ---
61
62                  int i; // Laufzahl für for-Schleife
63
64                  for (i=0; i<12; i++)
65                  {
66                          if (gspeed_measured >= tt_n[i] &&
                                gspeed_measured <= tt_n[i+1])
67                          {
68                                  a_interpol = tt_m[i+1] -
                                        tt_m[i];
69                                  b_interpol = tt_n[i+1] -
                                        tt_n[i];
70                                  c_interpol =
                                        gspeed_measured - tt_n[
                                        i];
71
72                                  torque_rated = a_interpol/
                                        b_interpol*c_interpol +
                                         tt_m[i];
73                          }
74                  }
75
76
77                  // --- PITCHGAIN-ABFRAGE ---
78
```

```
79                  int k; // Laufzahl für for-Schleife
80
81                  for (k=0; k<4; k++)
82                  {
83                          if (pitch1_measured >= gain_angle[k
                                ] && pitch1_measured <=
                                gain_angle[k+1])
                                        {
84                                  a_interpol = gain_factor[k
                                        +1] - gain_factor[k];
85                                  b_interpol = gain_angle[k
                                        +1] - gain_angle[k];
86                                  c_interpol =
                                        pitch1_measured -
                                        gain_angle[k];
87                                  gain1_kp = (a_interpol/
                                        b_interpol*c_interpol +
                                         gain_factor[k]) * 1/ci
                                        ;                   }
88                  }
89
90
91                  int m; // Laufzahl für for-Schleife
92
93                  for (m=0; m<4; m++)
94                  {
95                          if (pitch2_measured >= gain_angle[m
                                ] && pitch2_measured <=
                                gain_angle[m+1])
                                        {
96                          a_interpol = gain_factor[m+1] -
                                gain_factor[m];
97                          b_interpol = gain_angle[m+1] -
                                gain_angle[m];
98                          c_interpol = pitch2_measured -
                                gain_angle[m];
99
100                         gain2_kp = (a_interpol/b_interpol*
                                c_interpol + gain_factor[m]) *
```

```
                    1/ci;
101                 }
102             }
103
104
105             // --- PITCH-CONTROL ---
106
107             e_pitch_alt = e_pitch;
108             e_pitch = gspeed_measured - gspeed_rated;
109
110             pitch_demand1_alt = pitch_demand1;
111             pitch_demand2_alt = pitch_demand2;
112
113             pitch_demand1 = pitch_demand1_alt +
                    kp_pitch/gain1_kp * e_pitch + kd_pitch
                    *(e_pitch - e_pitch_alt)/ci;
114             pitch_demand2 = pitch_demand2_alt +
                    kp_pitch/gain2_kp * e_pitch + kd_pitch
                    *(e_pitch - e_pitch_alt)/ci;
115
116             if (pitch_demand1 <= 0)
117             {pitch_demand1 = 0;}
118
119             if (pitch_demand2 <= 0)
120             {pitch_demand2 = 0;}
121
122
123             // --- PITCH-TEETER-KOPPLUNG ---
124
125             pitch_teeter1 = pitch_demand1 - ppk*
                    teeter_angle;
126             pitch_teeter2 = pitch_demand2 + ppk*
                    teeter_angle;
127
128
129             // --- WERTUEBERGABE AN BLADED ---
130
131             SetDemandedGeneratorTorque(scd,
                    torque_rated);
```

```
132                     SetDemandedPitchAngle(scd, 0, pitch_teeter1
                            );
133                     SetDemandedPitchAngle(scd, 1, pitch_teeter2
                            );
134
135
136                     // --- BEENDEN DER SCHLEIFE ---
137
138                     return GH_DISCON_SUCCESS;
139             }
140 }
```

Bibliography

[1] *Condor Wind Energy.* http://www.condorwind.com/our_technology.html. – accessed 02-Nov-2014

[2] *HAW Hamburg - ZOFF.* http://www.haw-hamburg.de/?id=29891. – accessed 12-Jan-2015

[3] *FKM-Richtlinie - Rechnerischer Festigkeitsnachweis fuer Maschinenbauteile aus Stahl, Eisenguss- und Aluminiumwerkstoffen.* VDMA Verlag GmbH, 2002

[4] Adam, Mario: *Statistische Versuchsplanung und Auswertung (DoE Design of Experiments).* http://mv.fh-duesseldorf.de/d_pers/Adam_Mario/a_lehre/am_pflicht/0_DoE_Vorlesung_Skript_aktuell.pdf. – accessed 07-Aug-2014

[5] aerodyn engineering gmbh (Hrsg.): *Internal documents.* Buedelsdorf, Germany: aerodyn engineering gmbh, 2014

[6] Burton, Tony ; Sharpe, David ; Jenkins, Nick ; Bossanyi, Ervin: *Wind energy - handbook.* 1. edition. 2001

[7] Dvorak, Paul: *Teetering toward two-blade turbines.* http://www.windpowerengineering.com/design/teetering-toward-two-blade-turbines/. – accessed 08-Jan-2015

[8] Gasch, Robert ; Twele, Jochen ; Gasch, R. ; Twele, J. ; Bade, Peter ; Conrad, Wolfgang ; Heilmann, Christoph ; Kaiser, K. ; Kortenkamp, Ruediger ; Kuehn, Martin ; Langreder, W. ; Liersch, Jan ; Maurer, J. ; Ohde, Karsten ; Reuter, A. ; Schubert, Mathias ; Sundermann, Bastian ; Stoffel, Alexander: *Windkraftanlagen - Grundlagen, Entwurf, Planung und Betrieb.* 8. edition. 2013

[9] GL Garrad Hassan (Hrsg.): *Bladed external controller user manual.* Bristol, England: GL Garrad Hassan, 2013

[10] GL Garrad Hassan (Hrsg.): *Bladed Theory Manual Version 4.4*. Bristol, England: GL Garrad Hassan, 2013

[11] GL Garrad Hassan (Hrsg.): *Bladed User Manual Version 4.4*. Bristol, England: GL Garrad Hassan, 2013

[12] Glasgow, John C. ; Corrigan, Robert D.: Results of Free Yaw Tests of the Mod-0 100-Kilowatt Wind Turbine / U.S. Department of energy - Conservation and Renewable Energy - Wind Energy Technology Division. 1983. – Forschungsbericht

[13] Haibach, E.: *Betriebsfestigkeit: Verfahren und Daten zur Bauteilberechnung*. 3. edition. Berlin Heidelberg : Springer Science and Business Media, 2006

[14] Hansen, Carsten: *Aerolastic load simulation of a 3 MW two bladed wind turbine*, HAW Hamburg, Diplomarbeit, 2014

[15] Hansen, Martin O. L.: *Aerodynamics of Wind Turbines*. 2. edition. London : Earthscan, 2008. – ISBN 978–1–84407–438–9

[16] Hau, Erich: *Windkraftanlagen - Grundlagen, Technik, Einsatz, Wirtschaftlichkeit*. 4. edition. Berlin Heidelberg : Springer Science and Business Media, 2008. – ISBN 978–3–540–72150–5

[17] Henderson, G. M. ; Haines, R. S. ; Quarton, D. C.: The analysis and design implications of pitch-teeter coupling / Wind Energy Group Ltd, Garrad Hassan Partners. 1989. – Forschungsbericht

[18] International Electrotechnical Commission (Hrsg.): *Wind turbines - Part 1: Design requirements Third edition*. Geneva, Switzerland: International Electrotechnical Commission, 2005

[19] Koehler, M. ; Jenne, S. ; Poetter, K. ; Zenner, H.: *Zaehlverfahren und Lastannahme in der Betriebsfestigkeit:*. 1. edition. Berlin Heidelberg : Springer Science and Business Media, 2012

[20] Koepp, Paul: *Turbine-maker Nordic Windpower files for liquidation bankruptcy*. `http://www.bizjournals.com/kansascity/print-edition/2012/10/19/turbine-maker-nordic-windpower-files.html`.
Version: 2012. – accessed 12-01-2015

[21] Kost, Christoph ; Mayer, Johannes N. ; Thomsen, Jessica ; Hartmann, Niklas ; Senkpiel, Charlotte ; Philipps, Simon ; Nold, Sebastian ; Lude, Simon ; Schlegl, Thomas: Stromgestehungskosten Erneuerbare Energien

Studie / Frauenhofer-Institut fuer solare Energiesysteme ISE. Freiburg, 2013. – Forschungsbericht

[22] Manwell, James F. ; McGowan, Jon G. ; Rogers, Anthony L.: *Wind Energy Explained - Theory, Design and Application*. 2. edition. New York : John Wiley and Sons, 2009. – ISBN 978–0–470–01500–1

[23] Pesnel, Pierre: *The 1 MW WTG from Vergnet reveals features*. `http://proceedings.ewea.org/ewec2009/proceedings/statscounter.php?id=2&IDABSTRACT=427`. Version: 2009. – accessed 12-Jan-2015

[24] Quell, Peter: Vergleich von starrer und Pendel-Rotornabe fuer eine Windkraftanlage der Megawatt-Leistungsklasse am Beispiel der WKA Autoflug A 1200. In: *DEWEK'96-Tagungsband* (1996)

[25] RN-Wissen: *Regelungstechnik*. `http://rn-wissen.de/wiki/index.php/Regelungstechnik#Die_Regelstrecke`. – accessed 01-Nov-2014

[26] Schorbach, Vera ; Dalhoff, Peter: Two bladed wind turbines: antiquated or supposed to be resurrected?

[27] Schorbach, Vera ; Dalhoff, Peter ; Gust, Peter: Taming the inevitable: significant parameters of teeter end impacts.

[28] Schorbach, Vera ; Dalhoff, Peter ; Gust, Peter: Two bladed wind turbines - Undetermined for more than 30 years. In: *Proceedings of 8th PhD Seminar on Wind Energy in Europe* (2012)

[29] Schorbach, Vera ; Haines, Roger ; Dalhoff, Peter: Teeter end impacts: analysis and classification of most unfavourable events. In: *Wind Energy* (2015)

[30] Spera, David A.: *Wind turbine technology - Fundamental concepts of wind turbine engineering*. 2. edition. 2009

[31] Witcher, D. ; Lupton, R. ; Nim, E. ; Bossanyi, E. ; Nichols, J. ; Sun, Y.: *Bladed multibody validation*. Bristol, England: GL Garrad Hassan, 2011

Hochschule für Angewandte Wissenschaften Hamburg
Hamburg University of Applied Sciences

Erklärung zur selbstständigen Bearbeitung einer Abschlussarbeit

Gemäß der Allgemeinen Prüfungs- und Studienordnung ist zusammen mit der Abschlussarbeit eine schriftliche Erklärung abzugeben, in der der Studierende bestätigt, dass die Abschlussarbeit „– bei einer Gruppenarbeit die entsprechend gekennzeichneten Teile der Arbeit [(§ 18 Abs. 1 APSO-TI-BM bzw. § 21 Abs. 1 APSO-INGI)] – ohne fremde Hilfe selbständig verfasst und nur die angegebenen Quellen und Hilfsmittel benutzt wurden. Wörtlich oder dem Sinn nach aus anderen Werken entnommene Stellen sind unter Angabe der Quellen kenntlich zu machen."

Quelle: § 16 Abs. 5 APSO-TI-BM bzw. § 15 Abs. 6 APSO-INGI

Dieses Blatt, mit der folgenden Erklärung, ist nach Fertigstellung der Abschlussarbeit durch den Studierenden auszufüllen und jeweils mit Originalunterschrift als letztes Blatt in das Prüfungsexemplar der Abschlussarbeit einzubinden.
Eine unrichtig abgegebene Erklärung kann -auch nachträglich- zur Ungültigkeit des Studienabschlusses führen.

Erklärung zur selbstständigen Bearbeitung der Arbeit

Hiermit versichere ich,

Name: Carstensen

Vorname: Torben

dass ich die vorliegende Masterarbeit bzw. bei einer Gruppenarbeit die entsprechend gekennzeichneten Teile der Arbeit – mit dem Thema:

Design and optimization of a pitch-teeter coupling and the free teeter angle for a two-bladed wind turbine to reduce operating loads.

ohne fremde Hilfe selbständig verfasst und nur die angegebenen Quellen und Hilfsmittel benutzt habe. Wörtlich oder dem Sinn nach aus anderen Werken entnommene Stellen sind unter Angabe der Quellen kenntlich gemacht.

- die folgende Aussage ist bei Gruppenarbeiten auszufüllen und entfällt bei Einzelarbeiten -

Die Kennzeichnung der von mir erstellten und verantworteten Teile der Masterarbeit ist erfolgt durch:

Hamburg		
Ort	Datum	Unterschrift im Original